FYSK04 Bachelor's degree project

Sugar-assisted transfer printing of K-Type TFTCs onto fiberglass laminate

Author
Maksymilian Zaluski

Supervisor
Anders Mikkelsen

Co-Supervisor
Ajša Ćuprija

LUND UNIVERSITY

Division of Synchrotron Radiation
Project period: 3 months

Abstract

As we have become more modern, we have become more reliant on electronic devices, containing micro- and nanosize components. Coming along with more advanced and complex manufacturing methods have become more advanced, they bear plenty of inconveniences, most commonly the impossibility of printing on surfaces with arbitrary surface curvature. This issue is resolved by the reflow transfer printing method, where the reflow ability of sugar is exploited to adapt to substrates with arbitrary curvature.

In the present project, the reflow transfer printing was studied with K-type thin film thermocouples (TFTCs) on fiberglass laminate substrates.

Two differently manufactured TFTC samples were studied, where a 5 nm nickel layer was pre-deposited, once in a different and once in the same depositing process.

During the experimental phase, several errors with damage and adhesion of the thin films were encountered. It turned out that the samples suffer from mechanical or chemical changes during the coating or baking step. Likely, stress on the thin film due sugar dehydration was the dominant aspect for component deformation and breaking.

Additionally, samples respective to separate deposition processes witnessed chemical changes after NiO formation between nickel/nickel alloy interfaces, due to stronger polar bond formation.

It is suggested that internal residual stresses have additional contribution on observed delamination of the thin films.

Regardless, six transfers were completed with various amounts of components transferred, as the TFTCs were subject to displacement and breaking. Still, the method has proven itself to be a functioning method to transfer alumel-chromel TFTCs onto non-flat composite surfaces, creating a base for a sustainable and innovative component transfer method.

Acknowledgments

Before this paper begins, I would love to note some acknowledgments.

Without the introduction to this project by my thesis supervisor Professor Anders Mikkelsen, I would have never expected this research field to exist. His introduction to the topic gave me the opportunity to discover this field and conduct research in this field on my own. Thanks to his problem solving knowledge and expertise, I was able to continue when I faced errors with my results during early stages of the project.

Above all, I want to express large gratefulness to my co-supervisor Ajša Ćuprija. Without her specific knowledge in the field, this project would not have gone forward. Thanks to her sharing her experiences on the method, I was capable of starting and conducting my own work. On top of that, she was the main provider of the material, which was crucial for any work done throughout this project. Ajša introduced me to the lab and all the equipment and was the primary contact for results and issues.

In addition, I am grateful to have Yash Velaveti working simultaneously with me on this project. Issues encountered during the experimental phase would not be able to resolved, if our cooperation and joined problem solving ability did not exist. Regularly maintained contact between both of us kept us up to date on each others experiences, complications and observations.

At this point, I also want to express my thanks to MyFab and NanoLund, providing the facility and equipment, making this research possible in first place.

Not to forget, I owe a mention to all my friends, family, acquaintances and, above others, my partner, supporting me throughout this project and my studies.

Contents

List of abbreviations

etc. = Et cetera

et al. = Et alia

i.e. = Id est

TFTC = Thin Film Thermocouple

EUV = Extreme Ultraviolet Lithography

EBL = Electron Beam Lithography

NIL = Nanoimprint Lithography

PDMS = Polydimethylsiloxane

EMF = Electromotive force

SEM = Scanning Electron Microscope

SE = Secondary electrons

BSE = Backscatter electrons

AFM = Atomic Force Microscope

D.I. = de-ionized

IPA = Isopropyl alcohol

PVD = Physical Vapor Deposition

NaCl = Sodium-chloride

NiO = Nickel-oxide

Cr_2O_3 = Chromium-oxide

Al_2O_3 = Aluminum-oxide

SiO_2 = Silicon-dioxide

SiOH = Silicon-hydroxide

1 Introduction and aim

Electronic devices have a big contribution to everyday life nowadays. Their components mostly include micro- and nanoscale parts or circuit boards coated with micro- and nano-electronics. However, micro- and nano-sized components usually require challenging approaches to production, usually due to lithographic or other production methods. This limits the components to being manufactured on perfectly flat wafers.[1] As a consequence, a completely flat component can make the application in electronics inconvenient, or particularly challenging, for instance in biomedical research[2] or in applying sensors onto composite surfaces for industrial and engineering purposes.

The constant need for micro- and nano-electronics in the last decades has led to a rapid development in fabrication techniques. Apart from large scale fabrication methods, researchers found several methods to transfer microelectronics onto surfaces with various shapes and flexibility.[3, 4] Among others, transfer printing became a common technique to transfer electronics. Based on the key idea of transferring electronic components, so called inks, from a donor substrate, or any alternative functioning wafer, onto a different receiving acceptor substrate, the transfer is done with the assistance of a stamp, a separate transfer medium.[3–5] However, for a long time transfer printing still faced inconveniences and complications. Mainly, the limitations in printing large structures and printing hard-to-access areas on the acceptor substrate limited its application.[1, 2, 4]

Recently, in 2020, when a group of scientists under T. Hong et al. (2020) proposed a new transfer medium to carry out transfer printing: sugar.[6] Not only does the application of sugar exclude various harsh chemicals, but also brings the advantage of effortless dissolution in water. Moreover, transfers onto flat and flexible substrates without damaging the transferred electronics appeared enormously successful.[6]

Shortly after, G. Zabow (2022) optimized transfer printing with sugar and revealed his new method of reflow transfer printing for three dimensional surfaces.[1] By adding corn-syrup to the sugar-water solution, he managed to find a suitable transfer medium for reflow based transfer printing. Since corn-syrup reduces the crystallization, it reduces the risk of damaging micropatterns. Zabow's method still excludes strong chemicals after adding corn-syrup and also allows flexible printing on difficult accessible, uneven and shaped microscopic surfaces with the sugars reflowability.[1, 4] As Zabow discovered the reflow transfer printing method, he achieved major successes with the reflow transfer method in practical application: As for demonstrating purposes, Zabow succeeded in transferring gold nanoarrays onto microscopic substrates, such as the tip of a needle, a red blood cell, poppy seeds and pollen.[1] Consequently, this method might offer new opportunities for science, industry and technology in the near future.[7]

Hence, the purpose of this Bachelor's thesis project is to apply Zabow's reflow transfer method, with the aim to extend the application knowledge of the method on industrial, non-flat receiving substrates. For this reason, the transfer onto composite fiberglass laminate was practiced throughout this project. Furthermore, as a base for possible future industrial and scientific applications, the focus lay in transferring K-type thin film thermocouple (TFTC) sensors on the chosen substrate. Subsequently, the samples undergo careful characterization with tools such as optical microscopy, scanning electron microscopy and atomic force microscopy to investigate the limitations of reflow transfer printing. The overall goal of the project is to test and improve the method beyond current literature.

2 Theoretical background

2.1 Lithography

With the advancement of small scale electronics, their respective components have become smaller, making microfabrication methods more complex. Also, a growing demand for small scale components is arising, needing mass-fabrication possibilities.[4] With time, plenty of fabrication methods are developing, adapting to the demand and manufacturing challenges. Most commonly, lithographic approaches, namely photolithography.[8]

While photolithography is a very common practice for patterning wafers nowadays[8, 9], it faces a lot of inconveniences. The main problems with photolithography are the requirement of high temperatures, high-energy radiation and aggressive chemicals[9], which might impact the quality of the substrates negatively.[6, 9] In photolithography, substrates are coated with several metal layers. On top of that, a photoresist is applied and exposed to radiation through a photomask.[8, 10] The photomask contains the wanted pattern of the components. Depending on the applied photoresist, the substrate is left with the photomask pattern.[8, 10] Very commonly, the substrates go through chemical etching in order to dissolve leftover photomask from photolithography processes.[10] Especially when patterning silicon wafers, which are very widely used as substrates, chemicals like hydrofluoric acid are frequently applied.[8] Even though it faces plenty of inconveniences, photolithography is still widely applied.[8] Especially extreme ultraviolet lithography (EUV) has become the primary way to print microcircuits and semiconductors.[10] What makes EUV special over other photolithography methods is the application of ultrashort wavelengths, resulting in high photon energy. Wavelengths on such a short scale usually require a laser plasma source and series of fine mirrors, able to focus and reflect the extreme ultraviolet beam.[10]

Similar issues hold for other types of lithography. Electron beam lithography (EBL), for example, has the advantage of not requiring a photomask, allowing direct printing of thin patterns onto the substrate.[8, 11] Yet, EBL still requires photoresists, high energy and voltage to operate.[11] As a result, the operation of EBL might become expensive and still subject to chemical etching. Moreover, the largest conventional problem with industrial manufacturing methods is the limitation to perfectly flat wafers.[1] For large scale printing, the wafers must be perfectly flat, allowing coatings to be evenly applied.[8]

As time progressed, researchers have discovered methods that are able to avoid some problems that modern photolithography faces. This includes nanoimprint lithography (NIL)[9] or soft lithographic approaches, such as transfer printing.[3, 4]

NIL is based on shaping structures using pre-fabricated molds onto substrates. Here, the mold contains the respective pattern that is supposed to be printed on the substrate.[11] Beforehand, the substrate is coated with a resist layer, allowing the resist to shape to the mold, during a solidification process. Most common solidification processes applied are heat and UV-radiation[8, 11], melting resist to fit the mold's shape. After applying a hardening technique, the mold can be removed from the substrate, leaving a printed substrate.[8, 9, 11] NIL gives the major advantages of printing large areas[11] on an economically friendly basis, reducing excess application of chemicals.[9] Since this method has been published, it found major use in manufacturing organic optoelectronic devices.[9]

On the other hand, transfer printing is based on transferring already existing electronics printed on a working donor substrate onto a different acceptor substrate.[3, 4] Transfer

printing is widely applied to transfer integrated devices, such as bio-integrated electronics and various sensors.[3] As an example, a success of transfer printing in the field of medicine, is the transfer of various sensors to a heart catheter. Apart from that, transferring transistors, LEDs, solar cells, etc. on different substrates has widely been achieved with transfer printing.

As mentioned in the introduction, the so called ink is transferred with the help of a stamp, being the transfer medium. Existing examples for stamps previously used in transfer printing are balloon stamps[2], usually made out of elastomer materials like polydimethylsiloxane (PDMS).[3, 4] Unfortunately, those stamps are often not able to reach areas with high curvature of substrates.[2]

The limitations of printing on highly curved substrates were recently fixed by implementing sugar as stamp instead.[1] The reflowability of caramelized sugar bears the physical advantage of adapting to arbitrary shapes when in a viscous state.[2] On top of that, the application of sugar maintains the possibility of transferring large scale patterns.[2, 6]

Above others, sugar is chemically harmless, very affordable and rather simple to purchase and handle. Since the publication of the reflow transfer method, further researchers have made use of the reflow transfer method in their research. Aside of the successes Zabow achieved. Examples of the successful applications of reflow transfer printing are the transfer of humidity and pressure sensors onto fabric substrates[7] or in the creation of silver nanoparticles.[12] The latter shows the variety of applicable sugars by choosing maltose as transfer medium.

Therefore, improvement and success of this method could open new possibilities in plenty of research fields, such as biomedicine, allowing the printing of live saving tools onto equipment, and optoelectronics, where transfer of solar cells could lead to a sustainable solution for consumer energy.[2–4] With relation to this project, the possibility of printing electronics onto composite material in general, could benefit manufacturing and operation of airplanes and cars.[13] Another notably important field is industry, where a success in transfer printing of TFTCs onto curved industrial manufacturing devices, creates a possibility of optimizing manufacturing processes, providing ecological sustainability in industry. An example of those industries makes tool manufacturing, where metal processing decides upon product quality.[14]

2.2 Properties of sugar

Sugars have the natural ability to form a solid structure[15] and additionally, the significant ability to undergo a phase change from that solid state to a more viscous state at certain temperature. This so called glass transition temperature, T_g, is unique for various types of sugar and depends on the chemical and physical properties of the respective sugar type.[16] Such properties are mainly the amount of water and molecular weight that the sugar contains.[17] The so called glass state is the equivalent to an amorphous state. The main property of an amorphous state lies in the disorganized atomic structure of the respective substance.[18] This results in a lower packing fraction of amorphous solids[17], which provides amorphous sugar its brittle property.

Caramelization describes the event of multiple reactions caused by heating sugar.[17] The longer sugar solutions are heated, the more differently it affects T_g. In the example of sucrose, T_g drops in the beginning, followed by an increase in T_g with time.[17] The de-

crease has to do with sucrose splitting into smaller compounds, i.e. fructose and glucose, with characterized lower T_g. At later stages, the molecules start forming chains due to polymerization, increasing the molecular weight and hence having an increasing effect on T_g.[17]

Generally, sucrose is among others one of the sugars with a low T_g.[17] However, sucrose has a higher T_g compared to other common sugars as fructose and glucose, according to Ruiz-Cabrera and S.J Schmidt (2015).[16] Based on their assumption, the increased T_g of sucrose is due to its higher molecular weight compared to fructose and glucose.

Another trait of sugars is their ability for crystallization under certain conditions. With relation to that, the research of J. Chen et al. (2015) has proven that the addition of corn-syrup reduces the crystal growth in regular sucrose.[19] The crystal growth rate enormously decreased with higher amounts of corn-syrup. Therefore, addition of corn-syrup to sugar provides an extra advantage in reflow transfer printing, as avoidance of crystallization avoids the damage to the transferred electronics.[1] Furthermore, adding corn-syrup to sucrose additionally decreases its T_g.[4]

2.3 Composite materials

Composite materials are characterized by their compositions of at least two other materials.[20, 21] The properties of the resulting composites are hence dependent on the combination and material properties of their base metals.[20]

Composites are manufactured by reinforcing a matrix base layer, with a second layer out of fibers, particles or flakes.[21] Common matrices used for composites are polymer, ceramic, carbon or metal based substances. Matrix reinforcing substances commonly applied are synthetics, such as glass or carbon, or natural organic fibers, originating from woods and leaves.[20, 21]

Enhanced properties include mechanical strength with relation to its weight, such as high stress and strain resistance and durability.[13, 21] Apart from mechanical advantages, thermal electric and magnetic properties[20] and chemical properties like corrosion resistance[13]are of major importance. This gives way for the applications in fields, ranging from aircraft and car part manufacturing to the biomedical and antenna devices.[13, 20]

A notable kind of composite is fiberglass. Fiberglass composite starts with a polymer based matrix, reinforced with glass-fibers.[13, 20] There exists multiple types of fiberglass composites, designed for distinct applications. Mixing the reinforcing fibers, provides fiberglass composites with, for example, high electrical and thermal resistivity, chemical resistance, strength and transparency. For that reason, fiberglass is often found in electrical application and car part production. Moreover, its production is uncomplicated, making it affordable.[13, 20]

2.4 The thermocouple

2.4.1 The physics of thermocouples

Thermocouple sensors are widely used for the measurement of temperature, especially in industry at high temperature exposure.[14, 22] Compared to regular household thermometers, thermocouples consist of two metal contacts responsible for the temperature

measurement.[23] Both metals are connected in one point, forming a hot junction, responsible for actual temperature measurements. In another point, a non-crossing cold junction exists, kept at constant temperature, responsible for measuring a resulting potential difference. Both junctions are crucial for temperature measurements respective to the Seebeck effect.[22, 23] The Seebeck effect describes the induction of an electromotive force (EMF) if both junctions register different temperatures.[22, 23] One junction is kept constant at room temperature. Meanwhile, the other junction is directly exposed to a different environment, with arbitrary temperatures. With increasing temperature difference between the connections, the Seebeck EMF increases together with current induced through the loop formed by the wires. The resulting voltage is then non-linearly dependent with relation to the temperature difference.[23]

Thin film thermocouples (TFTCs) are commonly applied based on their advantageous properties.[14] Aside of the steadfastness to high temperatures, TFTCs have the ability of being printed on curved and flexible surfaces.[14, 22] This gives major advantages over traditional wire based thermocouple devices.[22]

2.4.2 The fabrication of thermocouples

K-type TFTCs are widely made of nickel alloys, namely Chromel (NiCr) and Alumel (NiAlMnSi)[22], where the former is the K^+pole and the latter is the K^-pole, respectively.[14] Alumel and Chromel have the advantage of being very temperature resistant.[14]

The primary method for the deposition of TFTC contacts on silicon substrate are physical vapor deposition (PVD) techniques. Generally, PVD describes the deposition of metals onto substrates by ejecting atoms from a source.[24] The atoms then travel through a vacuum, finally hitting the sample. The shape of the TFTC is then determined by a mask placed on the substrate.[14]

For TFTC manufacturing, the common PVD techniques are thermal evaporation deposition[14] and sputtering.[22]

The concept of thermal evaporation deposition lies in heating a liquid metal to evaporation, causing it to release atoms.[24] Usually, the metal is heated with coils or an electron beam. A sample is directly placed above the metal source, allowing the evaporated metal to directly deposit itself on the sample.[24] Unfortunately, thermal evaporation deposition bears disadvantages for the deposition of thin films of alloys.[24] If the sample surfaces are colder, the deposited alloy may become faulty. Wetting, nucleation and cluster formation might be consequences of a temperature difference.[24] Another issue specific with alloys are varying melting temperature and evaporation temperatures of the individual alloy metals. This can result in one metal depositing first before another.[24]

The earlier mentioned disadvantages can be avoided by applying direct sputtering to the sample. Compared to thermal evaporation, the chamber is filled with an ionized gas, for example argon[22], which ejects the atoms from the metal.[24] The ejected atoms gain kinetic energy from the incident ions, launching them towards the sample surface. Since the atoms have relatively high energy, they are more likely to embed themselves in the sample surface. This avoids the major issues faced in thermal vapor deposition.[24]

Depositing thin films on a substrate can lead to residual stress due to thermal mismatches from the difference in specific heat capacities of substrate and thin film metal.[25, 26] Residual stress can cause damage and delamination of thin films.[25]

Apart from alumel's and chromel's high temperature resistance[14], those nickel alloys are high in stiffness, referring to Young's modulae of NiAl and NiCr, with $Y_{Al} \approx 186$ GPa and $Y_{Cr} \approx 206$ at room temperature, respectively[27], implying low deformability and brittle fracture.

Additionally, nickel and nickel alloys are able to form nickel-oxide (NiO) when exposed to oxygen.[28] Even though alumel and chromel thin films show vulnerability to corrosion, as research investigated when exposed to sodium-chloride (NaCl) solutions, both alloys formed their respective oxide layer.[28] Alumel showed increased amounts of corrosion damage, while chromel showed higher chemical resistance.

2.5 Atomic bonds

Metallic interfaces between identic or different metals are characterized by forming metallic bonds. These bonds are formed when free valence electrons bound with neighboring atoms. Metallic bonds are not arranged, allowing them to be ductile and letting them deform with application of pressure.[29, 30]

Polar bonds on the other hand form with relation to an increased difference in electronegativity of elements. They are a type of covalent bonds, as atoms do not get fully ionized, as they do in ionic bonds. Instead, electronegativity is the ability of an element to capturing electrons into its own valence shell. Oxygen, for example, is among the elements with highest electronegativity, providing a strong polar bonding ability with metals.[31, 32]

2.6 Scanning Electron Microscopy (SEM)

SEM is a way to investigate substances on the micro- and nanoscale. It has the ability to magnify individual particles[33], surface topography and morphology.[34] Images of sample surfaces can be produced at high resolution and used to investigate the composition of substances. Additionally, it can capture particle sizes at micrometer scale.[33] It is broadly used in many fields such as in characterization of nanoparticles[33] and characterization after tribological tests to sample surfaces, i.e. the change of a sample surface structure after impact of friction and wear.[35]

SEM does not operate like an optical microscope. Instead of a light beam, a high energy electron source directs a beam onto the sample surface.[34] Electrostatic lenses and apertures focus the beam on a chosen point on the sample.[33] That point is continuously scanned by the electron beam. The scanned images are stacked to form a sharp picture on the operating computer.[34] The smaller the scanned area, the higher the magnification that can be achieved.[35]

After the electron beam hits the sample surface, it scatters and reflects electrons.[34] Different kinds of detectors are responsible for detecting certain types of electrons.[33] Primarily, SEM detects secondary (SE) and backscatter electrons (BSE).[33, 34] SE's scatter off the sample surface after impact and get detected by sensors placed on the side of the sample.[34] The detection of SE allows high resolution of surface topography and is sensitive to small pieces, namely debris and abrasive particles.[35] BSEs are reflected electrons detected by sensors placed parallel to the electron beam.[34] Compared to SEs, BSEs are higher in energy and mass sensitive, allowing to separate the chemical composition of the substances.[34, 35]

To ensure a sharp image, the SEM chamber is kept under vacuum, reducing unwanted ionization between gases and electrons.[35] Additional vibration insulation keeps the image steady, reducing inaccuracies of the image.[33, 34] A disadvantage of SEM is that it does not reproduce colorful images.[35] Instead, SEM images reveal contrasts, depending on the observed sample substances.

2.7 Atomic Force Microscopy (AFM)

AFM is a tool to investigate the surface properties of substances.[33] It has a high resolution and accuracy on the nanometer scale, allowing to create three dimensional images of a substance.

Instead of measuring reflected or scattered rays like other types of microscopes do, AFM is a tip probe based tool, which scans the surface of the investigated substances.[33, 35] Therefore, a completely evacuated chamber is not necessary in AFM.[35] The tip is mounted onto a flexible lever, allowing it to adapt to the surface of the substance. The tip is able to measure the surface structure either by contact or non-contact based detection of the surfaces.[35] The height is measured by reflected laser beams from the lever, allowing highly accurate surface measurements.[33, 35] The height is then synchronized with the planar position of the tip probe, resulting in a three dimensional topographic map.[33]

Apart from height measurements, tapping mode has the ability of measuring changes in the tapping phase, allowing the measurement of surface chemistry of the substance.[36] Changes in tapping phase are caused due to the difference in initial tapping oscillation of the tip and the delayed release of the tip from the tapped surface area, due to different chemical properties of the substances, changing the oscillation of the tip. The brighter the phase image, the stiffer is the measured substance.[36]

AFM appears additionally useful in this project, as it detects thin films.[35] However, it bears the disadvantage of returning inaccurate substance magnifications, making it mainly useful for height difference measurements.[33]

3 Experimental method

Over a period of six weeks, the reflow transfer printing method was practiced on fiberglass substrates. The experiments were carried out in a clean-room to ensure an extra clean environment, reducing the exposure to unwanted particles. Prior to any experiment, a wet bench license and sufficient training were acquired ensuring minimum risks and errors when conducting the experiment. The transfer medium was prepared ahead of starting the experiment. Sugar, corn-syrup and deionized-water (D.I.) were mixed together in a 2:1:1 ratio[1] and following heated until caramelization. Here, each chip sample contains multiple TFTCs with varying sizes, as seen in Figure 1.

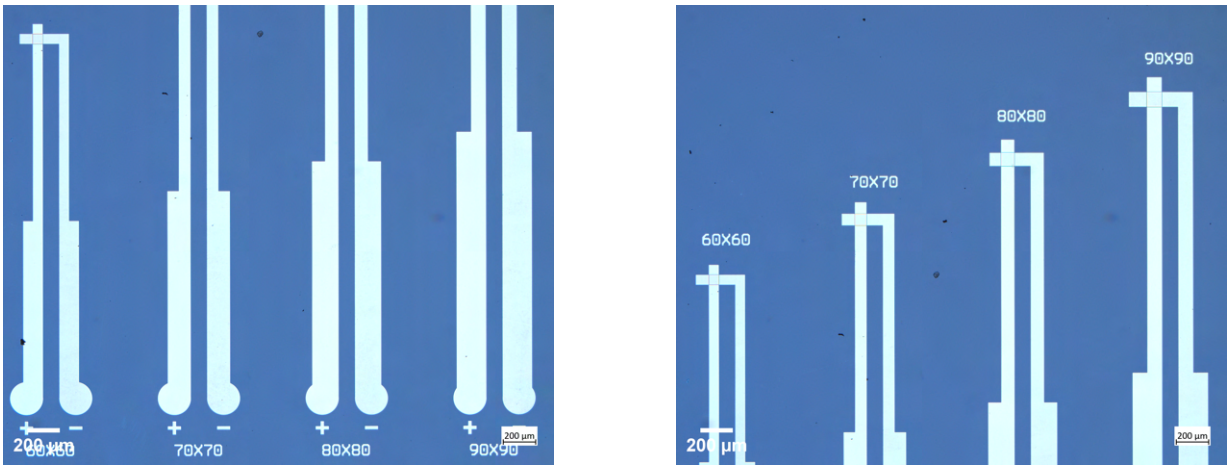

(a) Bottom side: cold junction.

(b) Top side: hot junction.

Figure 1: Example image of TFTCs sensors transferred in this project on silicon chip. Contacts on the left are the K^+poles (chromel) and contacts on the right are the K^-poles (alumel), respectively. Dark blue surface in the background is the silicon chip. Each sample chip contains TFTCs of five different sizes.

3.1 Preparation of the samples

During the experimental period, there have been two different K-type TFTCs studied in this project, subject to two different ways of manufacturing. Ahead of starting the experiments, they were pre-fabricated by the project co-supervisor, respectively.

The first and most studied TFTCs in this project were manufactured by firstly evaporating a 5 nm pure nickel layer onto a silicon wafer. In a separate sputtering process, the nickel alloys were sputtered with a thickness of 140 nm onto the silicon. The later TFTCs have been manufactured with the same material thicknesses. Different to the firstly manufactured TFTCs, the nickel layer and nickel alloys were deposited onto silicon in the same sputtering process.

Before coating the thermocouples with the sugar solution, the thermocouple samples were carefully sterilized with solvents, acetone and isopropyl alcohol (IPA), on the wet bench. Additionally, the acetone and IPA baths were placed in an ultra-sonic cleaner as an extra precaution for a clean surface. Afterwards, the samples were dried with a nitrogen (N_2) gun. This procedure is crucial to remove any organic residue on the samples [22], either caused by accidental contact with human skin or leftover residue from cutting the silicon wafer into individual chips.

Separately, identic sterilization was carried out on the receiving substrates. The sterilization of the receiving substrate is considered particularly important since the substrates were brought into the clean room from an outside environment.

3.2 Coating and baking of the thermocouples

Next, the sugar solution was carefully applied onto the thermocouple samples with the help of a pipette. Depending on the sample size, one to three drops of solution were enough to coat the whole electronic. During the experimental period the amount of sugar was more varied to see any difference in the lift-off success. Immediately after, the samples were

placed on a silicon wafer, to guarantee stability when placed in the oven, as seen in Figure 2a.

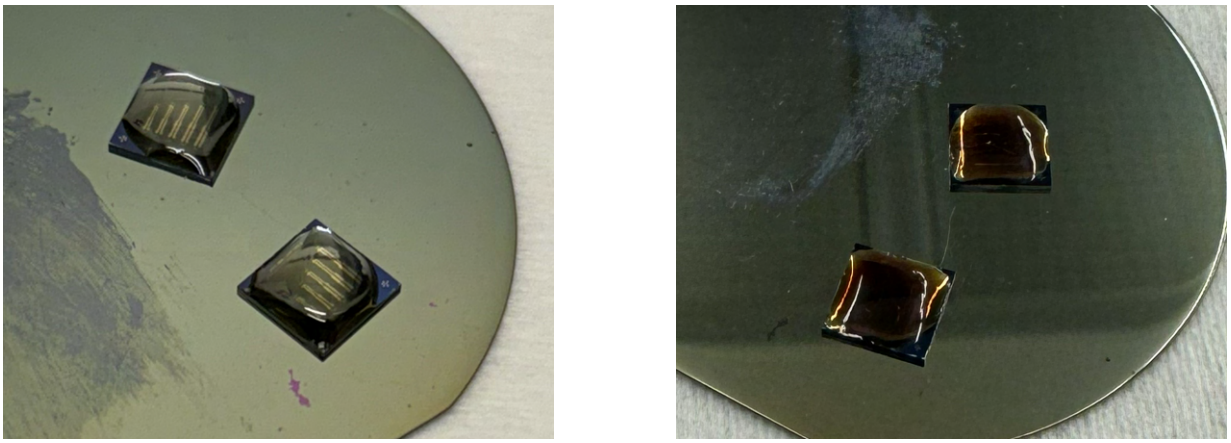

(a) Before baking

(b) After baking

Figure 2: Example TFTC samples, coated with an arbitrary amount of sugar, before baking (a) and after baking (a), both positioned on a silicon wafer. (a) shows the sugar solution in a viscous liquid state, where (b) shows the sugar in the solid state.

The baking step includes both the hardening and cooling of the sugar, resulting the samples as in Figure 2b. Heating the samples was sometimes done in steps until the oven reached the final baking temperature. A timer on the oven was set to a specific baking duration. Immediately after the timer ran out, the samples were left to cool down.

To optimize the experimental procedure, each of the first six experiments underwent different parameters in the baking process. All coating and baking parameters applied for each individual experimental attempt are described in detail in Table 1. At first, the avoidance of air bubble formation was highly prioritized[1], to avoid pattern disorganization. Therefore, the first and third attempts were subject to very slow heating steps to try avoiding bubble formation. In the third attempt the baking time was additionally reduced to 9.5 hours to see any differences in adhesion of the K^+/K^-poles. The slow heating attempts were compared to moderate heating attempts, with less steps, in the second and fourth experiments. Except of the third attempt, all samples were baked for 12 hours.

Finally, a fifth experiment was performed, without any heat applied. The sample was only left coated over 24 hours, to see if the liquid had any impact on the TFTC components. In a separate sixth experiment, the sample was then subject to baking, before it was coated with sugar, to again investigate any improvements in lift-off.

It is important to note that samples in experiments 7-10 were replaced by the most recently manufactured TFTCs. The heating gradient in experiments 7 and 8 was set to 5°C/min, following a baking time of 12 hours at 110°C and for experiments 9 and 10 to 4°C/min at 105°C for 12 hours. Their result was compared to the previously conducted experiments with the earlier manufactured samples.

The amount of coating applied on the samples was decided upon the sample size and improvements to previous experiments.

Table 1: Baking parameters, respective to each conducted experiment.

No.	Max. temp [°C]	Steps [°C]	Baking time [h]	Amt. sugar [drops]	Pre-baked [°C, hrs]	Transferred
1	110	30, 50, 60, 80, 100, 110	12	3 (long sample)	-	Yes
2	115	70, 115	12	2 (short sample)	-	Yes
3	100	30, 45, 60, 65, 70, 75, 80, 85, 90, 95, 100	9.5	3 (short sample)	-	No
4	110	60, 80, 110	12	2 (long sample, spread with pipette)	-	Yes
5	room temp.	-	24	2 (short sample)	-	No
6	110	-	12	2 (short sample)	60, 0.5	No
7	110	5°C/min	12	2 (short samples)	-	Yes
8	110	5°C/min	12	1	-	No
9	105	4°C/min	12	2	-	Yes
10	105	4°C/min	12	2	-	Yes

3.3 Lift-off and transfer

The following day, after the baked samples cooled down, the hardened sugar was lifted off the sensor sample. The samples were carefully secured with tweezers, while force was carefully applied with a scalpel from an opposite edge. Since the sugar resulted to be very brittle, one paid high attention to this process to avoid major cracks forming, which could complicate transfer or characterization steps. Additionally, the risk of damaging the sample was avoided by not applying too much pressure with the tweezers and scalpel. The result of an arbitrary lift-off step can be seen in Figure 3a. Subsequent to a successful lift-off step, the hard sugar and sensor sample were again investigated under optical microscopy to determine the success of their respective baking parameters.

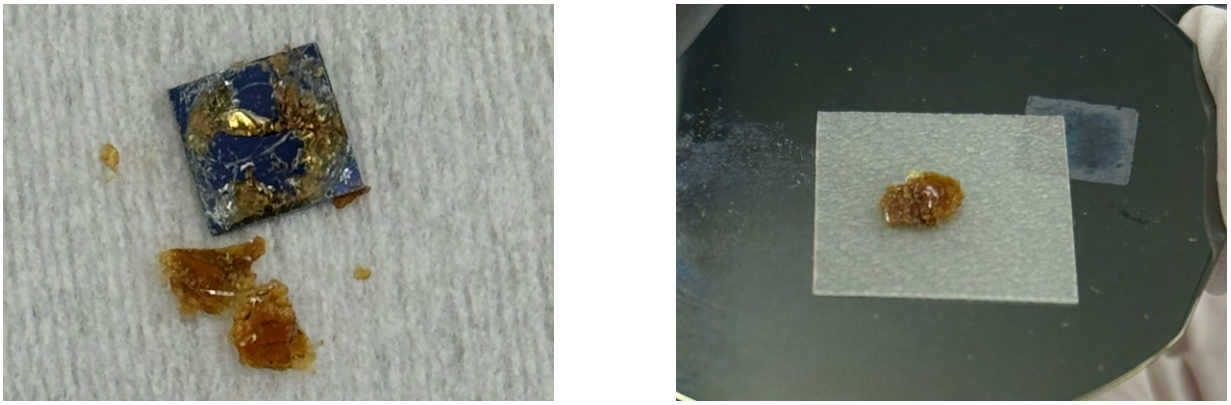

(a) Lift-off step

(b) Sugar placed on substrate

Figure 3: Example TFTC sample after lift-off (a) and the solid sugar placed on the receiving fiberglass substrate (b). The marks and strains on the silicon chip are leftover sugar and TFTC components. The hard sugar contains pieces of TFTC components.

To make use of the reflow ability of sugar, a hot plate was then used to re-heat the sugar on the respective substrate. For fiberglass substrates, a temperatures of 60-70°C turned out to be an appropriate choice. By poking the sugar in frequent intervals with a pair of tweezers, one determined if the sugar changed phase and already stuck to the substrate.

When that was the case, the substrate was finally transferred to a beaker with D.I water, until the sugar finally dissolved. The water from the beaker was slowly sucked up with thin strips of paper towels, ensuring minimal disorganization of the transferred sensor samples.

3.4 Microscopic characterization

To determine the microscopic success of the lift-off, the chips were subject to further characterization. Since optical microscopy bears the disadvantage of being too limited in its magnification ability, it was impossible to identify the different nickel layers of the TFTCs. Therefore, characterization tools like the Hitachi SU8700 SEM and Bruker AFM were applied for further investigation of the lift-off success of different TFTC component layers. The SEM electron beam was operated at an acceleration voltage of 5.0 kV and the AFM was operated in tapping mode. Their sensitivity gave the ability to investigate the silicon chips surface topography to spot further experimental results beyond the abilities of optical microscopy. SEM and AFM images were compared to each other to prove or disprove observations from optical microscopy. Beforehand, a license and required training for SEM were acquired.

4 Results and discussion

4.1 Experimental part

4.1.1 Sugar lift-off and microscopic characterization

During the experimental period, none of the necessary equipment was damaged, allowing an unproblematic execution of the experiments. One can observe partial lift-off results on all donor samples. Example images from the first chips, manufactured in separate sputtering processes, after lift-off are demonstrated in Figure 4

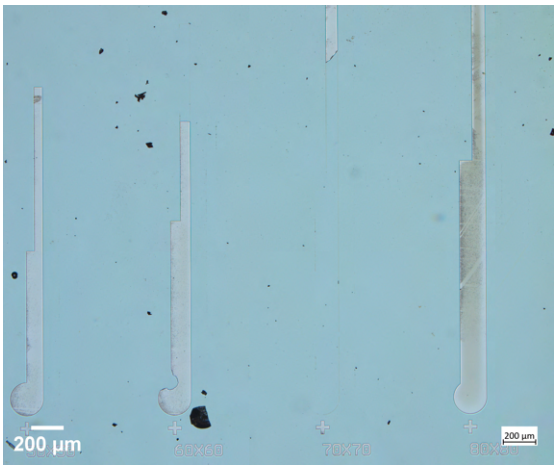

(a) First experiment: Silicon chip after lift-off.

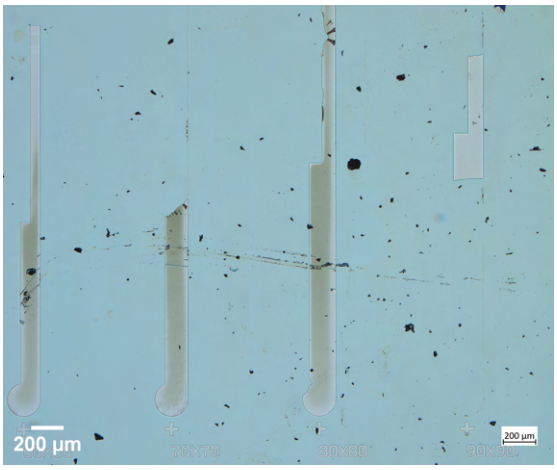

(b) Second experiment: Silicon chip after lift-off.

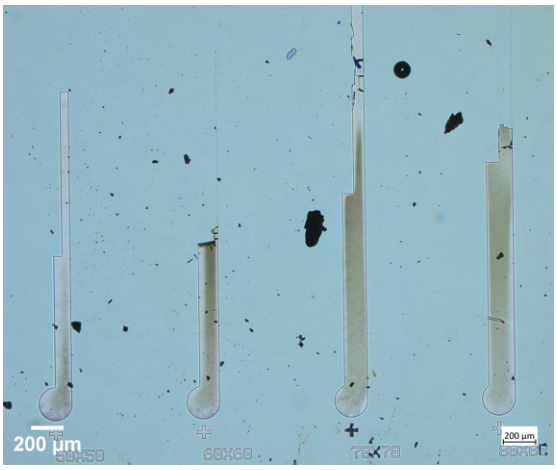

(c) Third experiment: Silicon chip after lift-off.

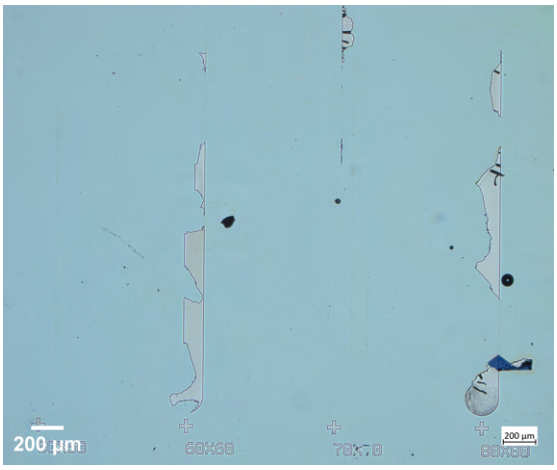

(d) Fourth experiment: Silicon chip after lift-off.

Figure 4: Example images of silicon chips with various amounts of TFTC residues after sugar lift-off step. Varying amount of residue shows different lift-off successes. Each picture represents one experimental attempt. (a,c) were subject to slow heating and a max. $T = 110$ and 100°C. (b,d) were subject to moderate heating at max. $T = 115$ and 110°C.

Here, the K^-poles completely lifted-off in every experiment, whereas the K^+poles were limited in their lift-off success or left behind more residue. Even in the third attempt, subject to very slow heating, high sugar moisture complicated the lift-off step, but Figure 4c confirms the lift-off of the K^-poles. High moisture content results in more adherent sugar, limiting sugar lift-off to thinner layers without components. As a result, enough sugar dehydration is necessary for a successful lift-off. The difference in lift-off for K^+/K^-poles implies an adhesion issue between the silicon surface and the nickel-alloys. Compared to slow heating (Figures 4a,4c), moderate heating in the second attempt (Figures 4b) benefited the sugar lift-off step and the lift-off of K^+ components by a small amount. Since most poles lifted off in Figure 4d, one can conclude that a high baking temperature and moderate heating with a moderate amount of sugar coating result in the best lift-off parameters.

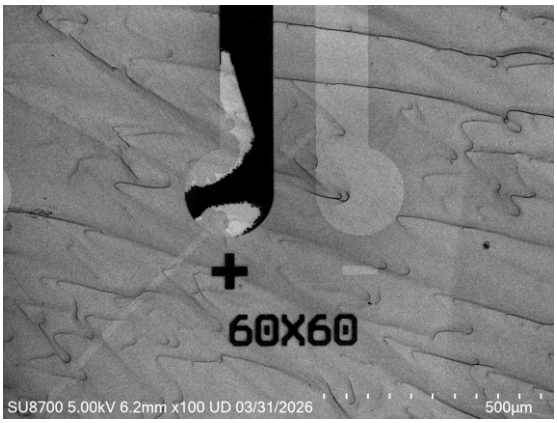

(a) SE

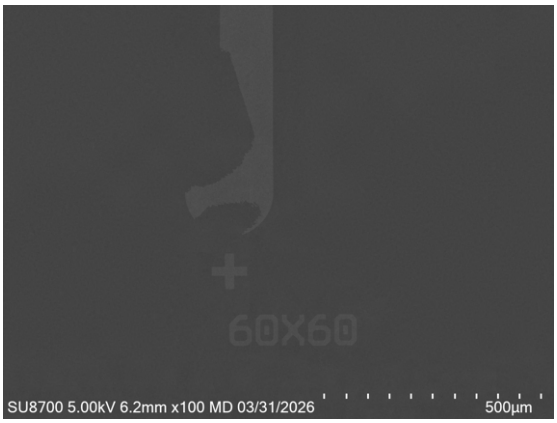

(b) BSE

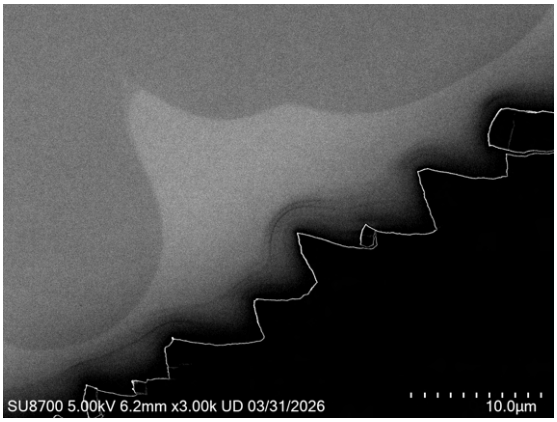

(c) SE

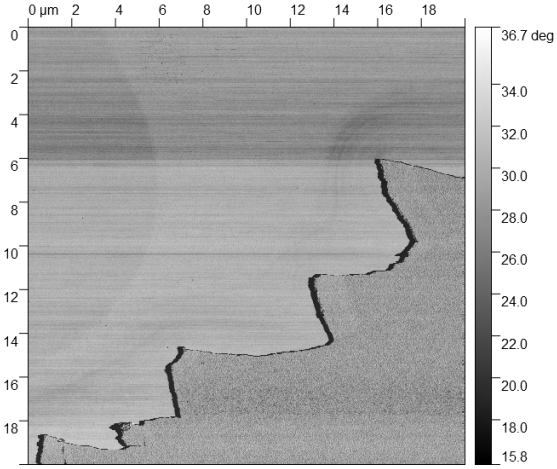

(d) AFM (phase)

Figure 5: SEM and AFM micrographs of the fourth experiment, subject to moderate heating in three steps. (a-b) portray the bottom side of the 60x60 μm TFTC. Both images represent the same point on the chip, comparing SE (a,c) and BSE (b) micrographs at a 5.0 kV acceleration voltage. (c-d) side-by-side comparison of SEM micrograph (c) and AFM phase image (d), where (c) represents a zoom-in view of the K^+pole shown in Figure (a). SE indicate layer residue after lift-off, while AFM phase determines the change in material properties of TFTC layers after lift-off.

After lift-off SEM shows the lift-off extend TFTCs from the fourth experiment, demonstrated in Figure 4d. The secondary electron (SE) and backscatter electron (BSE) micrographs in Figure 5 show layers of various microstructures left behind on the silicon chip. SE micrographs (Figures 5a, 5c) show more layers, due to SE's surface sensitivity[35], whereas BSE is higher in energy and mass sensitivity.[34, 35]

To complement these observations, this chip was additionally subject to AFM. As a result, the AFM phase image (Figure 5d) shows a different behavior of the tip towards the surface. The increase in brightness of the intermediate layer shows an increase in material stiffness[36], indicating presence of a pure nickel layer. AFM confirms lift-off of K^+poles happening in layers, possibly indicating a change in bonding behavior between the layers.

Since there is no height difference spotted in the height image between the chip and nickel layer, the nickel layer must be very thin. A side-by-side comparison between height and phase images can be found in Appendix A.

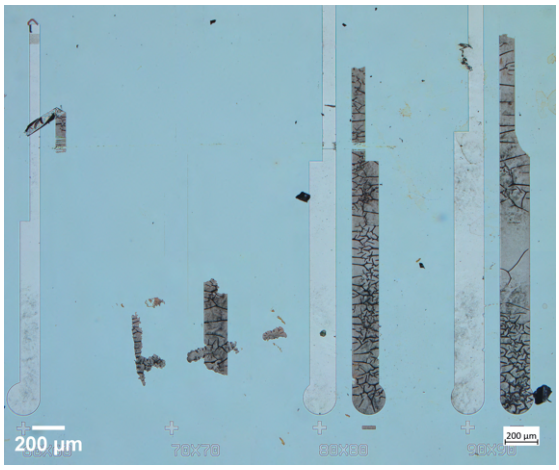

Figure 6: (a) Micrograph of silicon chip after the fifth experiment. This sample first was coated with the sugar solution and then placed in the oven at room temperature. The oven was shut-off, applying no higher temperature.

(a) SE

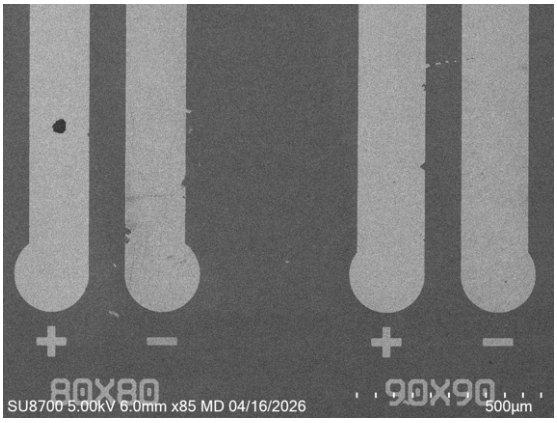

(b) BSE

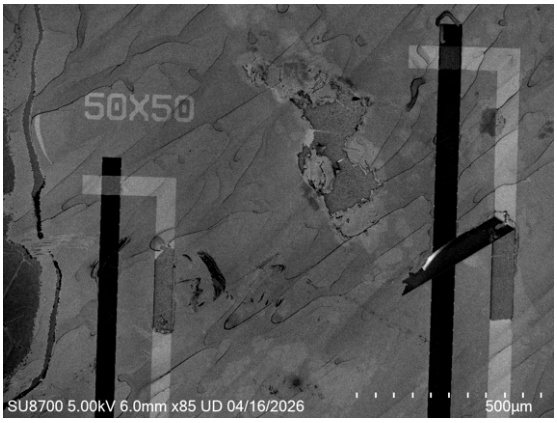

(c) SE

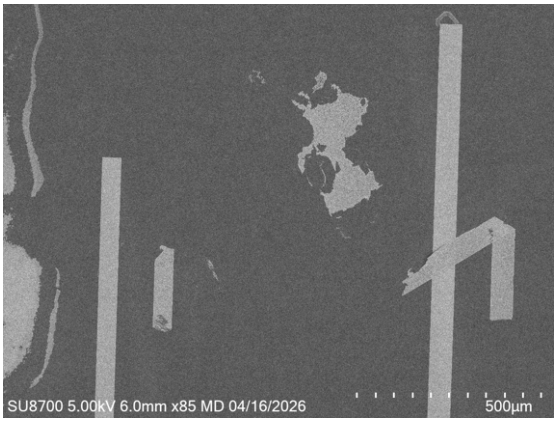

(d) BSE

Figure 7: SEM micrographs of the fifth sample. (a-b) represent the cold junction of large size TFTCs. (c-d) represent the measuring junction of small TFTCs. Both junctions are compared side to side by SE (a,c) and BSE (b,d).

The adhesion issue was confirmed in the fifth experiment, where a lift-off happened, even though no heat was applied in the baking process. Figure 6 shows similar occurrences as

in Figure 4, even though the sample was not exposed to any heat. Different to the chips in Figure 4, where K^-poles always lifted-off the chip, K^-poles in Figure 6 show crack and fold formation. SEM of the fifth sample (Figure 7) shows microcracks in the TFTC structures, which have formed while coated with sugar. Hence, the coating step itself must have led to delamination of the TFTCs. This observation raises the idea of chemical and mechanical occurrences affecting the quality of the TFTCs.

Additionally, over Figure 5 and 7 extending patterns and stripes stripes were determined not to be TFTC material but leftover residue from the sugar which might have not dissolved properly ahead of SEM characterization. Since just D.I. water was used for the dissolution, cleaning with acetone and IPA might solve this issue. In the present project, this was not done as the chips were not probed and were not subject to additional characterization.

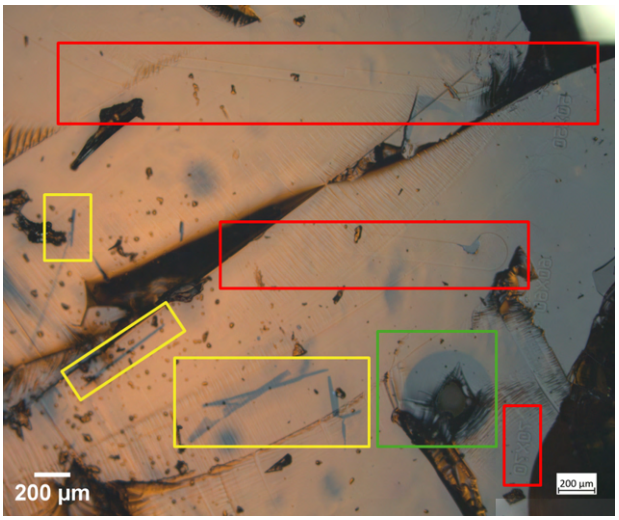

Figure 8: Micrograph of the hard sugar after the lift-off. Visible are shapes of the K^+poles molds (red), air bubbles (green) and TFTC components (yellow). Image represents first experimental attempt, subject to slow heating.

Optical microscopy of the hardened sugar revealed more details about the lifted-off TFTC component outcome. As an example, Figure 8 reveals significant dislocation of the lifted-off TFTC components in the sugar (yellow).

One possible reason extending the degree of displacement may be air bubbles or stresses due to dehydration, emerging during baking. Air bubbles have both been observed in Figure 8 (green) and by bare eyesight in almost all experiments. Since slow heating did not avoid air bubble formation, it appears likely that trapped air[1] or water vapor emerge.

Investigating further, Figure 8 (red) shows clearly visible patterns of K^+poles in the sugar, indicating the K^+poles molding onto the sugar. This confirms that only a limited amount of the K^+poles lifted-off in this case, as previously observed in Figure 4a. This was not only observed in the first experiment but in all experimental attempts of this project.

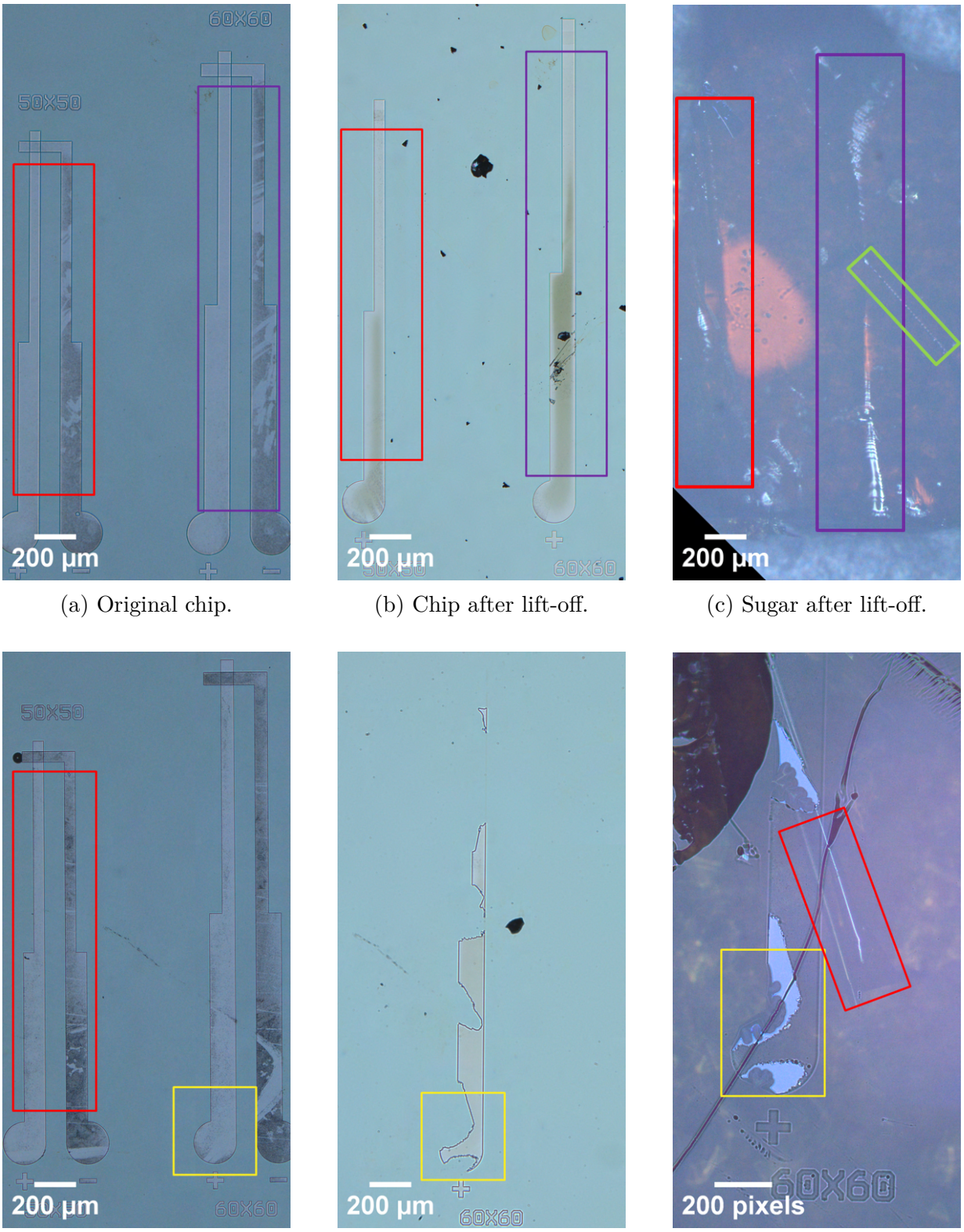

(a) Original chip. (b) Chip after lift-off. (c) Sugar after lift-off.

(d) Original chip. (e) Chip after lift-off. (f) Sugar after lift-off.

Figure 9: Lift-off micrographs of second experiment (a-c) and fourth experiment (d-f), both subject to moderate heating. Parallel aligned TFTC components found in the sugar after the lift-off, visible in Figures (c, f). Red and purple marked components are likely to be K^-poles of smaller TFTCs. Green marked components are likely to be displaced K^-pole of other TFTC on chip. Yellow marks lifted off 60x60 μm K^+pole components, which managed to stay in place and could be traced back to original contact.

Figure 9 portrays side-by-side comparisons of the identified pieces with relation to the silicon chip. Figures 9a-9c represent the second experiment and Figures 9d-9f the fourth experiment, which were both subject to moderate heating, with two and three heating steps. Inside the sugar, several straight aligned components were found (red/purple), which can be traced back to components on the original TFTCs with the help of after-lift-off micrographs. Simultaneously, some lifted off K^+pole parts (yellow) could be traced back to their original position on the chip, visible in Figures 9e-9f. The components in Figure 9f (red) resulted in a diagonally aligned position which could again be explained by observed air bubbles from the baking step.

In case of Figure 9c, the sugar thickness made it difficult to recognize more details. The thickness of the sugar layer resulted in a different brightness adjustment of the optical microscope, making it hard to focus on specific details.

Additionally, Figures 9c and 9f reveal more information about the outcome of the TFTC components. Different to Figure 8, closer analysis reveals that the components must be absorbed inside the sugar, instead of sticking to the sugar surface, as expected ahead of the experiment. This would additionally explain why some components appear twisted and wrinkled and leads to the overall observation of mechanical or chemical occurrences influencing the experimental result.

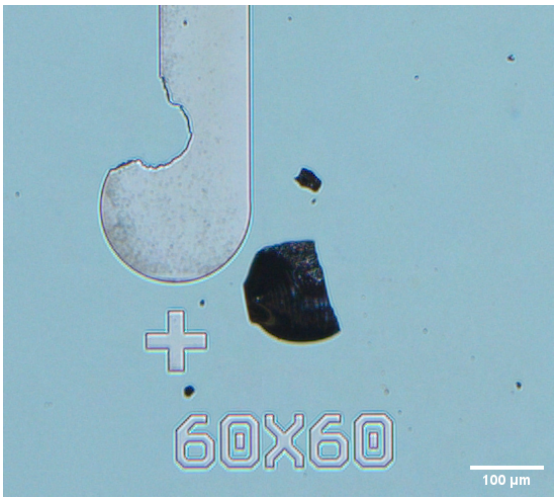

(a) Chip after lift-off

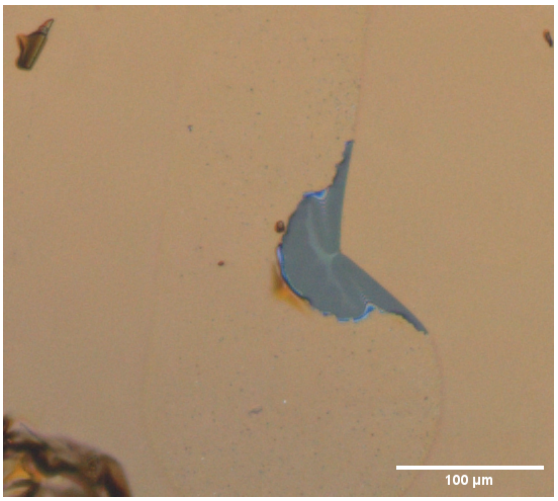

(b) Sugar after lift-off

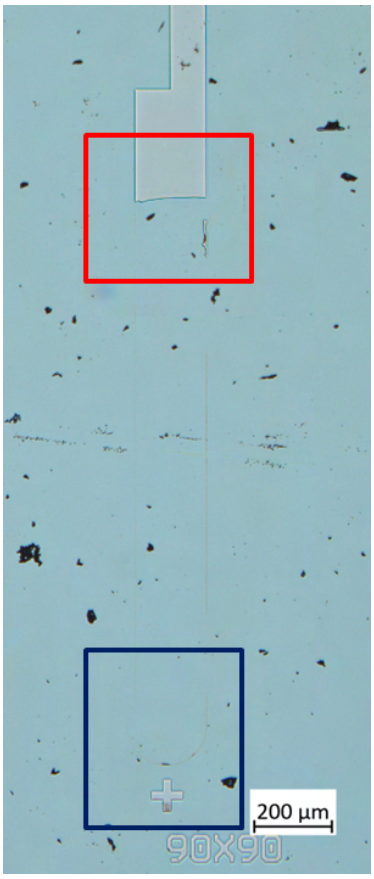

(c) Chip after lift-off

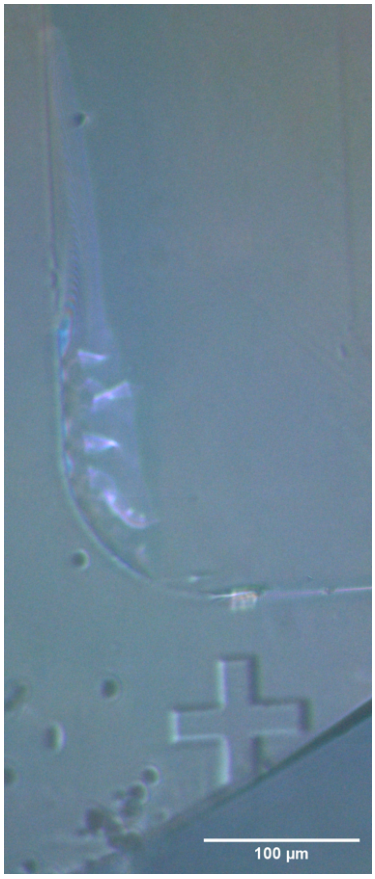

(d) Sugar after lift-off

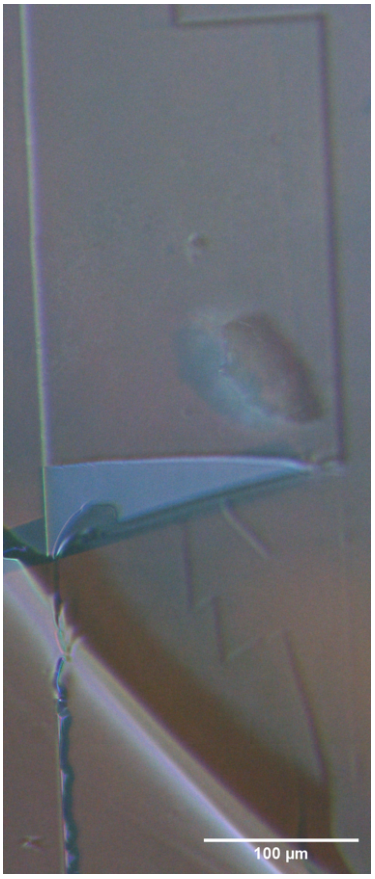

(e) Sugar after lift-off

Figure 10: Examples of identified K^+pole components of arbitrary TFTCs. (a) and (b) represent the first experiment, subject to slow heating, while (c-e) represent the second experiment, subject to moderate heating. Markers in (c) mark recognizable components in (d, blue) and (e, red).

Although, when K^+poles did manage to lift-off, they managed to stay in their place on the sugar, observed in Figures 9e-9f and 10. Sometimes, pieces as in those examples could be traced back to the original TFTC, as they seem not to have suffered from absorption.

Overall, a side-by-side comparison based on Figure 4 and Table 1 allowed to break down

the ideal parameters for most lift-off. Based on microscopic observations the fourth experiment turned out best in terms of lift-off quantity of both K^+ and K^-poles (Figure 4d). Breaking down the baking parameters, most components lifted-off at moderate heating with two or three temperature steps over baking time of 12 hours. It is difficult to say, if the variations made in the maximum baking temperature made any differences in lift-off variation. Clearly slow heating attempts made it difficult for the K^+poles to lift-off (Figures 4a,4c) and did not avoid bubble formation (Figure 8). Shorter baking times must be synchronized with the heating steps, as slow heating and shorter baking time led to too high moisture of the sugar, making it difficult to lift the sugar off in one piece (Figure 4c). Spreading less sugar coating with a pipette, reduces sugar thickness after baking, making hard sugar layer less brittle and easier to lift-off in practical terms, allowing better sugar lift-off.

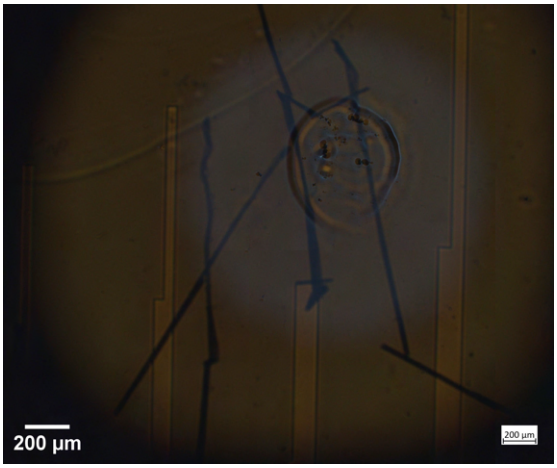

(a) Sixth experiment: Silicon chip before lift-off.

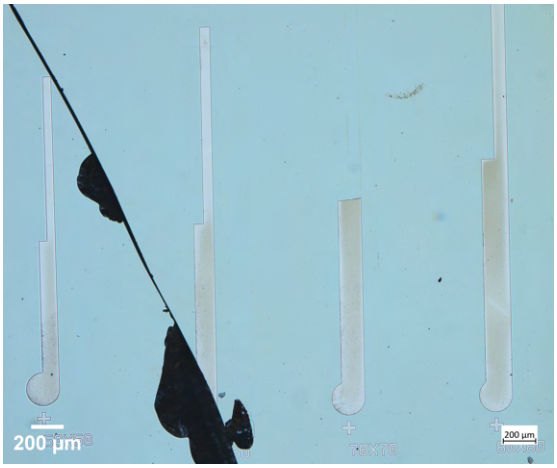

(b) Sixth experiment: Silicon chip after lift-off.

Figure 11: Micrographs of sixth TFTC sample with (a) and without (b) sugar, after baking step. This particular sample was pre-baked at 60°C for 30 minutes, before coating with sugar. The brightness of the (a) image was increased afterwards. The black line across the sample right marks a crack, that happened during lift-off.

Furthermore, in the sixth experiment a TFTC sample was subject to baking before coating. The goal of this attempt was to see if pre-baking at 60°C for 30 minutes would change anything in the adhesion and lift-off of the poles. Since annealing with heat is practiced in industry, to soften and reduce internal stresses from metals, one expected, that pre-baking would reduce internal stresses resulting from the TFTC manufacturing, giving better surface adhesion.[26, 37, 38] Also, heating reduces the Young's modulus of the alloys, making them softer.[27] Figure 11 shows final the behavior of the poles. Compared to results in Figure 8, here K^-poles keep their elongated shape, but still end up absorbed and wrinkled, while there is still limitations with the lift-off of K^+poles. The lift-off for this sample did not happen, as the chip cracked together with the majority of sugar. Though, pre-heating could be one way to reduce damage to the K^-poles.

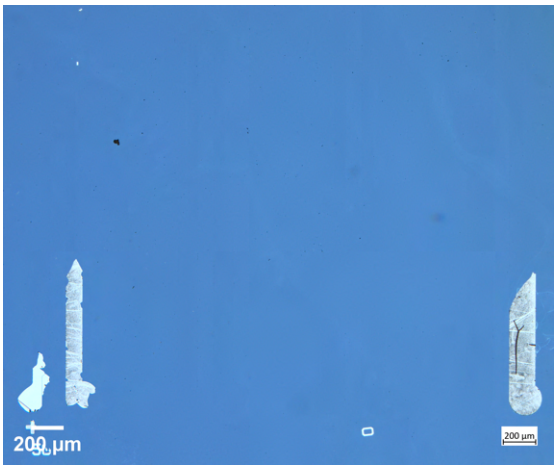

(a) Seventh experiment: Chip after lift-off.

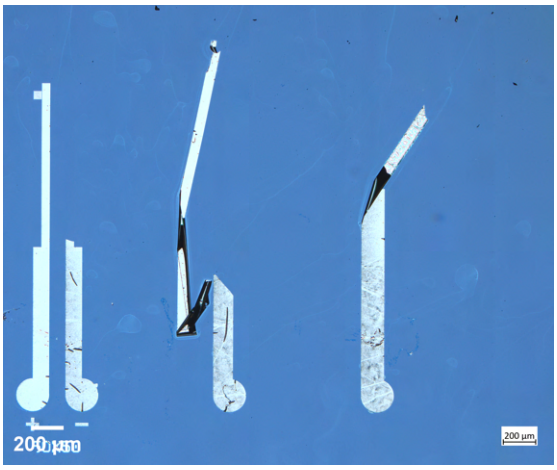

(b) Eighth experiment: Chip after lift-off.

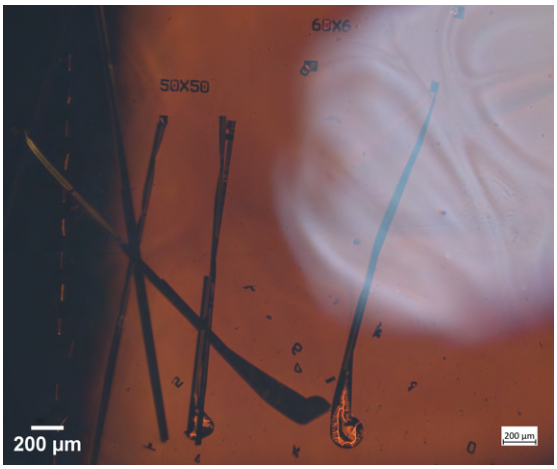

(c) Ninth experiment: Before lift-off.

(d) Ninth experiment: After lift-off.

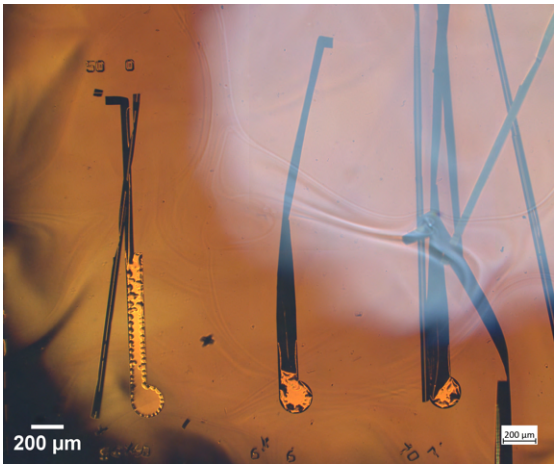

(e) Tenth experiment: Before lift-off.

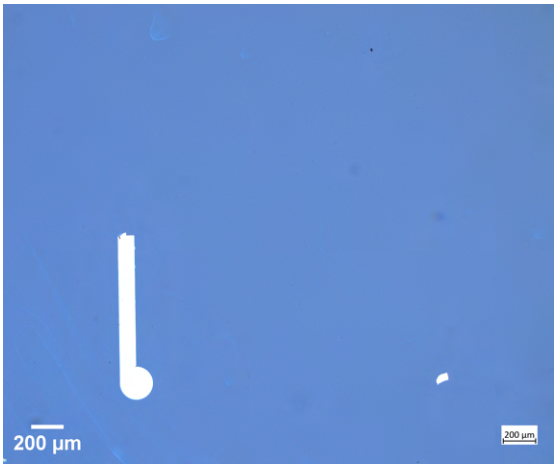

(f) Tenth experiment: After lift-off.

Figure 12: Micrographs of the seventh (a), eight (b), ninth (c-d) and tenth (e-f) samples after lift-off. Here, individual material layers were sputtered in the same process. (a,d,f) visualizes lift-off of almost all components.(b) visualizes delamination of K^-poles, while K^+poles mostly lifted-off. (c,e) show component displacement inside solid sugar.

The four final experiments were conducted on improved K-type TFTCs. The improve-

ment lies in the deposition of the pure nickel and nickel-alloy films in the same sputtering process. In this case, a higher number of K^+poles lifted-off from the chip. K^-poles still appear subject to delamination than the K^+poles, observed in Figure 12b. Nevertheless, almost all components lifted off the new sample chips, Figures 12a,12d and 12f, marking an improvement to the earlier manufactured samples, where nickel and nickel-alloy layers were deposited in separate sputtering processes. The eighth sample was coated with too little sugar, making a lift-off impossible and the sample not useful for a transfer. Here, the components did not suffer large damage from the sugar, since in Figures 12c and 12e the TFTC contacts are still recognizable, even as they lifted-off the chip and dislocated. In terms of baking steps, a difference between 4°C/min (Figure 12d,12f) and 5°C/min (Figure 12a,12b) is difficult to determine, since the final results appear of similar outcome.

4.1.2 Transfers onto fiberglass laminate substrate

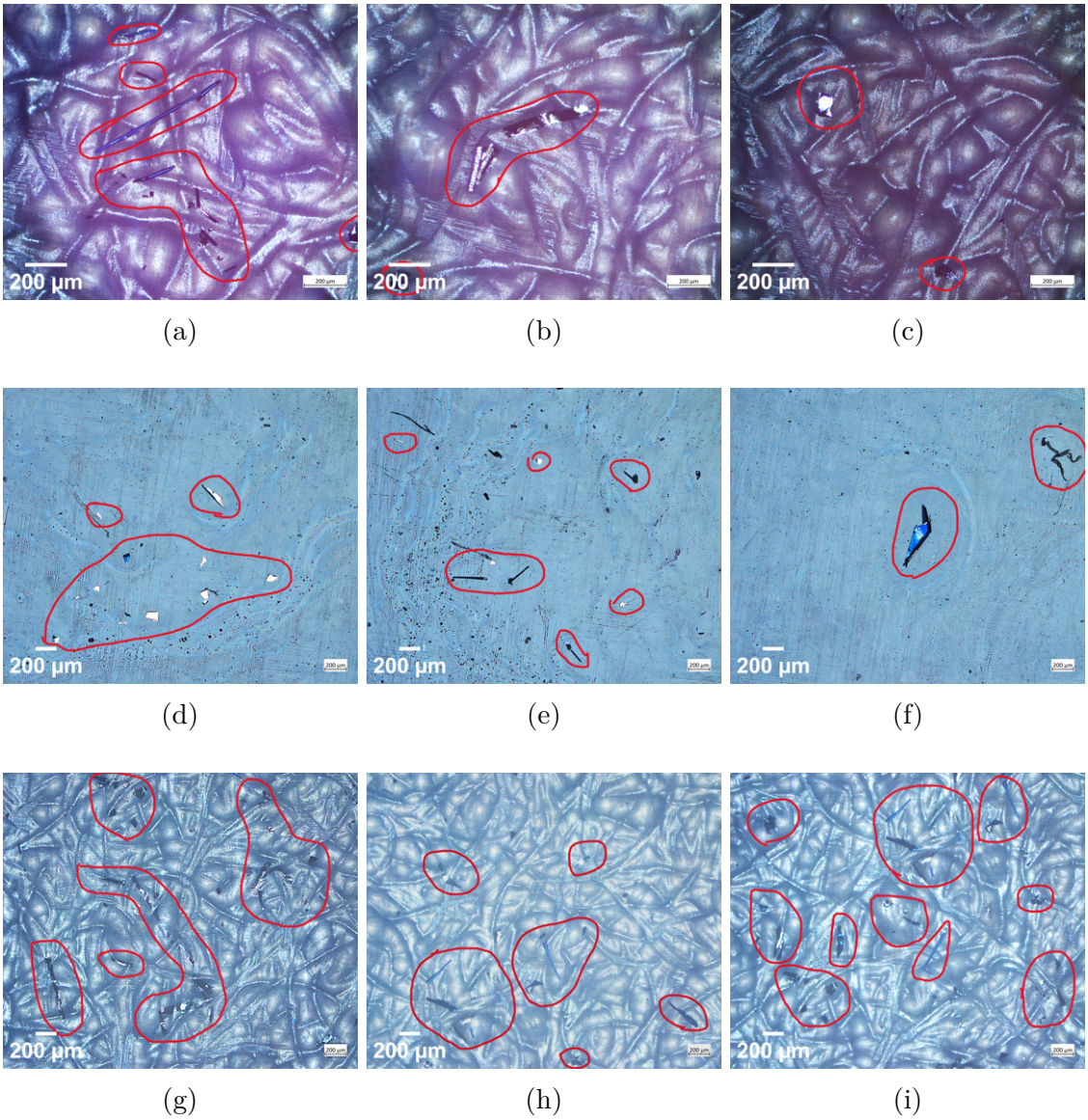

Figure 13: Micrographs of transfers completed initial TFTCs on fiberglass laminate substrate. (a-c), (d-f), (g-i) represent the first, second and fourth experiments, respectively. Visible on each micrograph are component debris from the TFTCs (red). Brightness, exposure and contrast were changed afterwards.

The micrographs in Figure 13 show the completed transfers onto fiberglass laminate substrates. Initially, successful transfers of some TFTC components can be identified on the fiberglass substrate. The transfer has worked both on the curved surface (Figures 13a-13i,13g-13i) and the flat surface (Figures 13d-13f) of the fiberglass substrate. Broken sensors from transfer and baking can be observed in all images in Figure 13. This may have been due to adhesion issues of the nickel alloys with silicon and absorption of components in the sugar. These observations again give clues about chemical or mechanical occurrences taking place during the experiment. From all samples, Figures 13g-13i show most components transferred, making the fourth experiment, subject to three heating steps, the best in terms of lift-off and transfer. Hence, moderate coating and heating, with 2-3 steps, and a long baking time ensure more K^+/K^-pole lift-off and transfer.

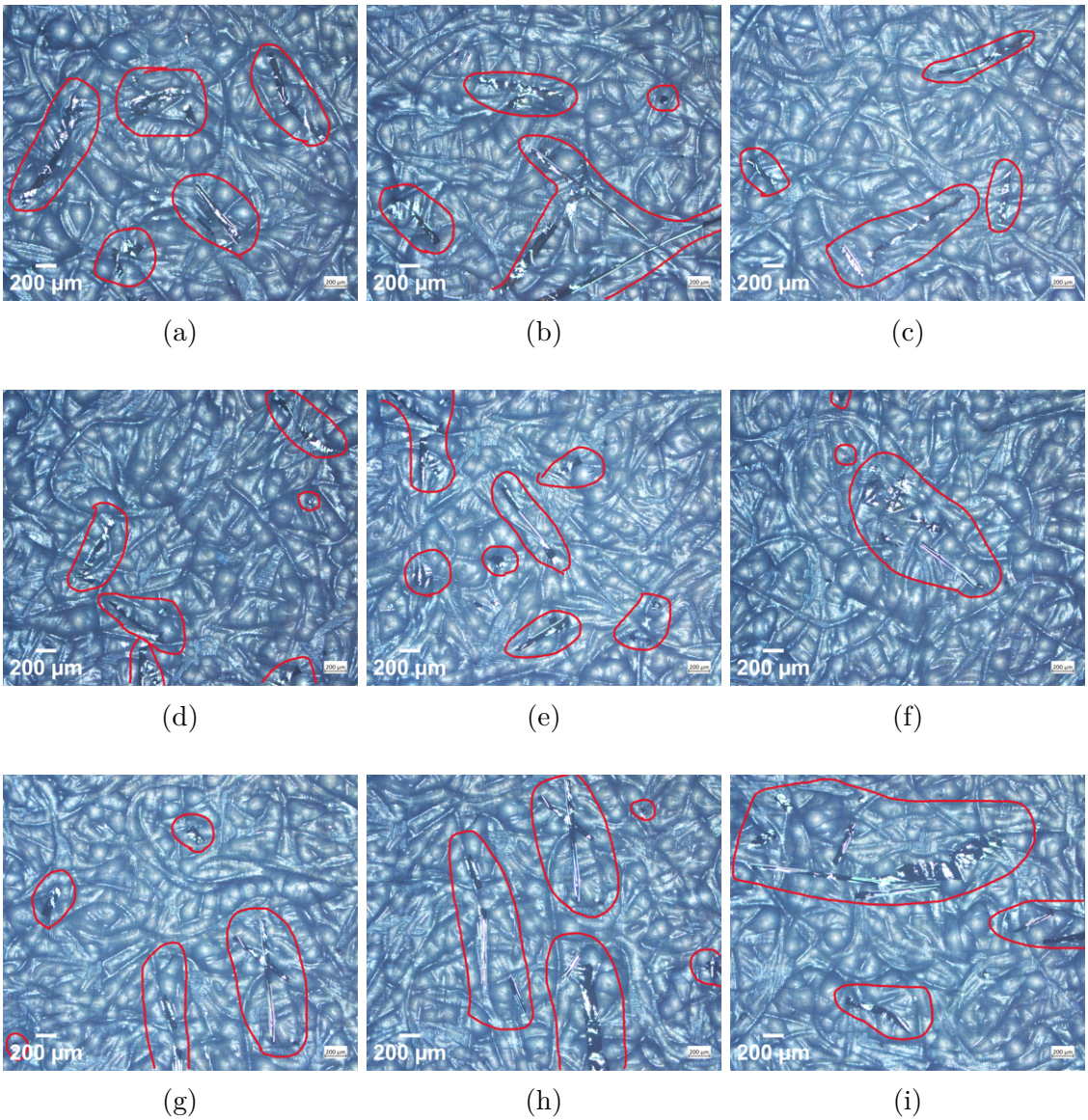

Figure 14: Micrographs conducted transfers from new sample batch onto fiberglass laminate substrate. Those transfers show components with least amount component damage, but maintaining high disorganization (red). Figures (a-c),(d-f),(g-i) represent the seventh, ninth and tenth experiments, respectively. Brightness, exposure and contrast were changed afterwards.

With the improved samples, whose TFTC layers were deposited in the same sputtering process, broken and displaced component pieces can be observed in Figure 14. Compared to Figure 13, larger components are more recognizable than in the previous attempts. Figure 14 shows improvement in terms of transferred component amount and quality. Especially components in Figure 14b appear to have kept most of their shape, making the fourth transfer (seventh experiment) the best in this project.

The absorption of the components by the sugar in the baking process made it impossible for the pattern to maintain its original shape. The pattern eventually moved around the fiberglass surface as the sugar was dissolved, which led to some of the parts getting lost in the water. Especially in the case of the second transfer experiment (Figure 13d-13f), the water was sucked out of the beaker too rapidly, leaving high displacement of the pattern and a lot of the parts getting lost. Therefore, keeping the speed of the water absorption low, reduced component displacement.

4.2 Discussion

In the earlier section, some mechanical and chemical occurrences were observed. Based on observations, those occurrences can be traced back to the sample coating or baking steps. As the baking process removes water from the sugar solution, the coating becomes harder as it dries. The TFTCs are likely to witness higher force from the dehydrated sugar coating than before, which would explain the deformation of the components.

Previous experiments revealed successful application of reflow transfer printing on samples with gold depositions with pre-evaporated nickel layers. Even though the final transfer marked displacement in the final pattern, issues with component absorption and lift-off issues, encountered in transferring alumel and chromel patterns, were not observed for gold. Moreover, the gold components did not break into small debris, as alumel and chromel components did in this project (Figures 13,14).

In addition, sensors were already successfully transferred with reflow transfer method. X. Chang et al. (2025) managed to transfer humidity and pressure sensors.[7] Notably, their sensors were made of gold depositions. No absorption issue was mentioned in their work.[7] Based on pure comparison, the sugar stamp provides better transfer results for gold depositions than nickel alloy depositions, but, a sacrificial layer maintained the overall shape of the sensor.

At first, a possible explanation might provide the difference in Young's modulae, Y, of the deposited materials. As gold has a lower Y compared to alumel and chromel, gold is more likely to deform under little pressure.[27, 39] This indicates that nickel alloys are likely to fracture if subject to too much force, rather than deforming, as gold does.

With relation to TFTC transfers, optical micrographs showed occurrences taking place with the absorbed contacts inside the sugar (Figure 8), especially for an increased amount of K^-poles. Y of alumel and chromel were compared with each other, based on existing literature, revealing that chromel has a minimally larger Y than alumel[27], signalizing higher deformability of alumel. The observations agree with the theory, as alumel contacts deformed more than chromel contacts (Figure 9). However, Y of alumel and chromel are still very similar to nickel, making the small difference in Y between the nickel alloys unlikely to have impact. Remark, the values compared are based on NiCr and NiAl, so one assumes their compositions to being mainly nickel based.

Experiments revealed that not only mechanical pressure is an issue. Figure 6 shows that the contacts delaminate without any heat applied, reducing baking stress on the samples. This introduces chemical changes or adhesive errors of the samples. Referring to theory, alumel and chromel are vulnerable to chemical damage in form of corrosion.[28] Especially alumel was observed to witness more corrosion damage. Based on present results in Figure 6, corrosion was initially suggested, since K^-poles showed delamination and flap formation, while the K^+poles were intact. However, thin films here were not subject to salty solutions, which excludes corrosion in the TFTCs.

With the exclusion of corrosion, account that the coated samples were only exposed to heat, air and the sugar solution. Also, it is highly unlikely for sugar crystals to damage the pattern, as corn-syrup reduces the crystallization of the solution.[1, 19] Regardless, SEM images in Figure 7 still show delamination and cracks of TFTC contact films. AFM (Figure 5d) shows layer residue after lift-off, indicating differences in adhesion and bonding, revealing the likelihood of chemical changes of the donors.

This project studied two differently manufactured TFTCs. The first batch of samples, respective to experiment one to six (Figures 4,6,11), had their nickel layer pre-deposited in an individual process, prior to the nickel-alloys. Removing the sample wafer from the evaporation chamber could have caused oxidation of the nickel, forming a nickel-oxide (NiO) layer.[28] Although separate literature has shown nickel and nickel alloys are very resistant to oxidation[40], a present NiO layer might impact adhesion properties, making nickel-alloy adhesion dependent on NiO interface, likely to happen in the first batch of samples.

The presence of oxygen in NiO might cause aluminum and chromium from the alloys to oxidize to Al_2O_3 and Cr_2O_3 at the NiO/alloy interface. Observations from the first batch of samples (Figures 4,6,11), chromel K^+poles showed limitations in lift-off, implying stronger bonding of Cr_2O_3 to NiO. Chromium-oxygen bonds are overall strong bonds[41], and oxygen can form strong polar bonds with metals.[31, 32] As a result, strong polar bonds are likely to form between NiO and Cr_2O_3/Al_2O_3 interfaces. Similar hexagonal corundum structures of Cr_2O_3 and Al_2O_3[41], imply similar strength, but, alumel contains only 2% of aluminum, while chromel contains a chromium share of 10%, allowing more Cr_2O_3 to bond between NiO and chromel. In addition, literature studying corrosion resistance of alumel and chromel films, shows Cr_2O_3 to be more stubborn against chemical changes, as it showed less corrosion damage to chromel films.[28] The polar bonds and resistance provided by the Cr_2O_3 layer between NiO and chromel (K^+poles) in the first sample batch (Figures 4,6,11), could explain the limitations in K^+pole lift-off from the first six chips.

In the new batch of samples (Figure 12), no NiO intermediate layer could form since the nickel layer was not exposed to oxygen, resulting in no Al_2O_3 and Cr_2O_3 formation. Since chromel and alumel consist of 90% and 95% nickel, one can assume metallic bonds to dominate the nickel/nickel-alloy interfaces. Likely, the polar oxygen bonds formed between NiO and Cr_2O_3/Al_2O_3 are stronger since metal-oxygen bonds are driven by high electronegativity differences.[31] Additionally, SiO_2 forming on the silicon is not reactive to nickel thin films.[42] Combined with the weaker metallic bonds, this could benefit the lift-off of the samples in the second batch (Figure 12). Non-existence of NiO would explain the improvement in overall lift-off and transfers for the recent batch of samples, in which metal layers were sputtered in the same process.

Apart from that, deposition and differences in the thermal expansion coefficients may cause

residual stress in the thin films, which benefits debonding.[38, 43] This means triggering a crack in the thin films, the inside stress will eventually drive further cracking. The presence of cracks or previous damage on the thin films, can cause SiO_2 to combine with humidity, which drives cracking, leading to debonding of thin film layers.[38, 43] SiO_2 bonds have the ability of absorbing water to form silicon-hydroxide (SiOH), needing more volume and thus increasing delamination driving stress[38], which would be accelerated by residual stresses. Alternatively, errors causing NiO formation at the SiO_2/nickel interface edge, could possibly cause debonding at the interface between films and silicon chip. Hence, this might explain delamination of thin films in the present results in Figure 6, where no additional heat was applied to the coated sample, and 12b. However, debonding occurrences have been studied for other thin films than nickel, deposited by chemical vapor deposition[38], not confirming these observations for sputter deposited K-type TFTCs.

5 Conclusion and future outlook

In conclusion, the execution of the reflow transfer method on K-type TFTCs unveiled difficulties and complications, since displacement and damage appeared in form of breaking and absorption of individual components. Analysis with microscopy helped to understand the occurrences, resulting in mechanical and chemical changes appearing during the coating and baking phase, as displacement, delamination and breaking of components was observed.

Testing the method on two differently manufactured samples led to different experimental outcomes of each sample batch. As the lift-off in the newer samples showed improved outcome, deposition of all layers in the same process shows experimental improvement. Non-existence of a NiO layer resulted in weaker metallic bonds, benefiting a lift-off of all poles from the chips (Figures 12a,12b,12d,12f). With the first samples, manufactured in separate sputtering processes, exposure to air formed NiO, allowing the formation of strong polar covalent bonds with Cr_2O_3/Al_2O_3. The higher amount of chromium in chromel allows more bonds with chemically resistant Cr_2O_3, resisting lift-off of K^+poles (Figures 4,6,11). Besides, delamination driven by residual stresses and liquid diffusion could cause additional damage to the thin films. However, this is unlikely, since this was not studied for identic samples but for other films and depositions.

Regardless, a significant amount of components was transferred on fiberglass substrate. The reflow transfer succeeded on both the rough and flat side of fiberglass laminate. With some improvement in adhesion between the thin films, the TFTC transfer on fiberglass can be completed.

In terms of future experimental improvement, a sacrificial layer between the sensors and chip might be a solution to avoid brittle sugar and damage to the components.[7] With relation to bubbles, a vacuum oven could help reducing bubble formation.[1] Alternatively, improving baking parameters, could help reduce further bubble formation or mechanical errors. Additionally, an investigation on the recently manufactured sample chips with energy dispersive spectroscopy or additional AFM, could reveal more about lift-off success and residue, compared to the earlier samples.

Even though the method itself is recent, the present work shows scientific success, particularly when improving of non-toxic methods. Throughout this project, no toxic chemicals were applied to complete transfers and the sugar and corn-syrup purchased in the super-

market are guaranteed to be harmless, since they are meant for oral consumption. Even though the present transfers did not turn out according to expectations, the accessibility of sugar, allows reflow transfers to be redone an unlimited number of times.

In summary, it is important to continue the research on reflow transfer printing, since production of microscopic components nowadays is unavoidable. As we are trying to become more sustainable in developing and manufacturing, reflow transfer printing could help us reach this goal soon. The combination of TFTCs and fiberglass opens doors for future studies and innovation[7] and improvement in existing application, production and research, crucial for the future.[13] The application of TFTCs may help adapting manufacturing and operation parameters to optimal conditions, allowing optimal and sustainable operations.[14]

References

[1] G. Zabow. "Reflow transfer for conformal three-dimensional microprinting (with supplementary material)". en. In: *Science* 378.6622 (Nov. 2022), pp. 894–898. ISSN: 0036-8075, 1095-9203. DOI: 10.1126/science.add7023. URL: https://www.science.org/doi/10.1126/science.add7023 (visited on 02/26/2026).

[2] Zhoulyu Rao et al. "Microprinting on curved surfaces with sugar". English. In: *Matter* 6.3 (Mar. 2023), pp. 671–673. ISSN: 2590-2393, 2590-2385. DOI: 10.1016/j.matt.2023.01.023. URL: https://www.cell.com/matter/abstract/S2590-2385(23)00049-8 (visited on 02/26/2026).

[3] Andrew Carlson et al. "Transfer Printing Techniques for Materials Assembly and Micro/Nanodevice Fabrication". en. In: *Advanced Materials* 24.39 (2012). _eprint: https://advanced.onlinelibrary.wiley.com/doi/pdf/10.1002/adma.201201386, pp. 5284–5318. ISSN: 1521-4095. DOI: 10.1002/adma.201201386. URL: https://onlinelibrary.wiley.com/doi/abs/10.1002/adma.201201386 (visited on 02/26/2026).

[4] Yiheng Li, Feilong Zhang, and Shutao Wang. "Regulatable interfacial adhesion between stamp and ink for transfer printing". en. In: *Interdisciplinary Materials* 3.1 (2024). _eprint: https://onlinelibrary.wiley.com/doi/pdf/10.1002/idm2.12139, pp. 29–53. ISSN: 2767-441X. DOI: 10.1002/idm2.12139. URL: https://onlinelibrary.wiley.com/doi/abs/10.1002/idm2.12139 (visited on 02/27/2026).

[5] Changhong Linghu et al. "Transfer printing techniques for flexible and stretchable inorganic electronics". en. In: *npj Flexible Electronics* 2.1 (Oct. 2018), p. 26. ISSN: 2397-4621. DOI: 10.1038/s41528-018-0037-x. URL: https://www.nature.com/articles/s41528-018-0037-x (visited on 02/26/2026).

[6] Tianzeng Hong et al. "Sugar transfer of nanomaterials and flexible electrodes". In: *International Journal of Smart and Nano Materials* 11.1 (Jan. 2020). _eprint: https://doi.org/10.1080/19475411.2020.1731622, pp. 1–10. ISSN: 1947-5411. DOI: 10.1080/19475411.2020.1731622. URL: https://doi.org/10.1080/19475411.2020.1731622 (visited on 02/27/2026).

[7] Xueyan Chang et al. "Thermal Reflow Transfer Printing of Ultra-Thin Metal Conductive Layer for Flexible Sensors on Fabric Substrate". In: *IEEE Sensors Journal* 25.13 (July 2025), pp. 23615–23622. ISSN: 1558-1748. DOI: 10.1109/JSEN.2025.3573715. URL: https://ieeexplore-ieee-org.ludwig.lub.lu.se/document/11023072 (visited on 02/27/2026).

[8] "Lithography and electrodes". en-US. In: *Chemical Solution Synthesis for Materials Design and Thin Film Device Applications*. Elsevier, Jan. 2021, pp. 277–307. DOI: 10.1016/B978-0-12-819718-9.00005-4. URL: https://www.sciencedirect.com/science/chapter/edited-volume/pii/B9780128197189000054 (visited on 03/02/2026).

[9] Ningning Song et al. "Nanoimprint Lithography Enabling High-Performance Organic Optoelectronics: Advances and Perspectives". en. In: *Nano-Micro Letters* 18.1 (Feb. 2026), p. 236. ISSN: 2150-5551. DOI: 10.1007/s40820-026-02093-z. URL: https://doi.org/10.1007/s40820-026-02093-z (visited on 03/02/2026).

[10] Dimitrios Kazazis et al. "Extreme ultraviolet lithography". en. In: *Nature Reviews Methods Primers* 4.1 (Nov. 2024), p. 84. ISSN: 2662-8449. DOI: 10.1038/s43586-024-00361-z. URL: https://doi.org/10.1038/s43586-024-00361-z (visited on 03/03/2026).

[11] Michael Wang, ed. *Lithography*. English. Accepted: 2023-12-01T14:07:11Z. IntechOpen, 2010. DOI: 10.5772/45639. URL: https://directory.doabooks.org/handle/20.500.12854/128908 (visited on 03/03/2026).

[12] Lu Chen et al. "Near-Theoretical Thermal Conductivity Silver Nanoflakes as Reinforcements in Gap-Filling Adhesives". en. In: *Advanced Materials* 35.31 (2023). _eprint: https://advanced.onlinelibrary.wiley.com/doi/pdf/10.1002/adma.202211100, p. 2211100. ISSN: 1521-4095. DOI: 10.1002/adma.202211100. URL: https://onlinelibrary.wiley.com/doi/abs/10.1002/adma.202211100 (visited on 02/27/2026).

[13] Puran Singh et al. "Composite material: A review over current development and automotive application". In: *Materials Today: Proceedings* (Nov. 2023). ISSN: 2214-7853. DOI: 10.1016/j.matpr.2023.11.012. URL: https://www.sciencedirect.com/science/article/pii/S2214785323050812 (visited on 04/29/2026).

[14] Dong Min Kim et al. "Optimal fabrication of a thin-film thermocouple (TFTC) using Alumel/chromel junctions". English. In: *Heliyon* 10.4 (Feb. 2024). ISSN: 2405-8440. DOI: 10.1016/j.heliyon.2024.e26128. URL: https://www.cell.com/heliyon/abstract/S2405-8440(24)02159-5 (visited on 03/19/2026).

[15] Jeong-Ah Seo et al. "The glass transition temperatures of sugar mixtures". In: *Carbohydrate Research* 341.15 (Nov. 2006), pp. 2516–2520. ISSN: 0008-6215. DOI: 10.1016/j.carres.2006.08.014. URL: https://www.sciencedirect.com/science/article/pii/S0008621506003946 (visited on 03/06/2026).

[16] M. A. Ruiz-Cabrera and S. J. Schmidt. "Determination of glass transition temperatures during cooling and heating of low-moisture amorphous sugar mixtures". In: *Journal of Food Engineering* 146 (Feb. 2015), pp. 36–43. ISSN: 0260-8774. DOI: 10.1016/j.jfoodeng.2014.08.023. URL: https://www.sciencedirect.com/science/article/pii/S0260877414003616 (visited on 03/06/2026).

[17] Bin Jiang et al. "Impact of Caramelization on the Glass Transition Temperature of Several Caramelized Sugars. Part I: Chemical Analyses". In: *Journal of Agricultural and Food Chemistry* 56.13 (July 2008), pp. 5138–5147. ISSN: 0021-8561. DOI: 10.1021/jf703791e. URL: https://doi.org/10.1021/jf703791e (visited on 03/09/2026).

[18] Jing Guo, Peng Liu, and X. -D. Xiang. "Decoding the glassy state: Ultrafast detection of amorphous liquid-solid transition". In: *The Innovation* (Jan. 2026), p. 101301. ISSN: 2666-6758. DOI: 10.1016/j.xinn.2026.101301. URL: https://www.sciencedirect.com/science/article/pii/S2666675826000482 (visited on 03/09/2026).

[19] Jiahui Chen et al. "State behavior and crystal growth kinetics of sucrose and corn syrup mixtures". In: *Journal of Food Engineering* 161 (Sept. 2015), pp. 1–7. ISSN: 0260-8774. DOI: 10.1016/j.jfoodeng.2015.03.032. URL: https://www.sciencedirect.com/science/article/pii/S0260877415001399 (visited on 03/24/2026).

[20] "Composites: Overview". en-US. In: (Jan. 2005), pp. 192–208. DOI: 10.1016/B0-12-369401-9/00545-3. URL: https://www.sciencedirect.com/science/chapter/referencework/pii/B0123694019005453 (visited on 05/04/2026).

[21] "Numerical modeling of hybrid composite materials". en-US. In: *Modelling of Damage Processes in Biocomposites, Fibre-Reinforced Composites and Hybrid Composites*. Woodhead Publishing, Jan. 2019, pp. 57–101. DOI: 10.1016/B978-0-08-102289-4.00005-9. URL: https://www.sciencedirect.com/science/chapter/edited-volume/pii/B9780081022894000059 (visited on 05/04/2026).

[22] Bekmurat Dalelkhan et al. “Advancing industry 4.0 with microfabrication of K-type TFTCs on stainless steel 316 L substrates: A study on SiO2 insulation, substrate thickness, and surface roughness optimization”. en. In: *The International Journal of Advanced Manufacturing Technology* 142.9 (Feb. 2026), pp. 4745–4757. ISSN: 1433-3015. DOI: 10.1007/s00170-025-17306-9. URL: https://doi.org/10.1007/s00170-025-17306-9 (visited on 03/19/2026).

[23] T.J. Bajzek. “Thermocouples: a sensor for measuring temperature”. In: *IEEE Instrumentation & Measurement Magazine* 8.1 (Mar. 2005), pp. 35–40. ISSN: 1941-0123. DOI: 10.1109/MIM.2005.1405922. URL: https://ieeexplore.ieee.org/document/1405922 (visited on 03/06/2026).

[24] S. M. Rossnagel. “Thin film deposition with physical vapor deposition and related technologies”. In: *Journal of Vacuum Science & Technology A* 21.5 (Sept. 2003), S74–S87. ISSN: 0734-2101. DOI: 10.1116/1.1600450. URL: https://doi.org/10.1116/1.1600450 (visited on 04/15/2026).

[25] Thomas R. Koenig et al. “The microstructural and stress evolution in sputter deposited Ni thin films”. In: *Surface and Coatings Technology* 412 (Apr. 2021), p. 126973. ISSN: 0257-8972. DOI: 10.1016/j.surfcoat.2021.126973. URL: https://www.sciencedirect.com/science/article/pii/S0257897221001468 (visited on 05/11/2026).

[26] *Residual Stresses in Thin Films Evaluated by Different Experimental Techniques — Springer Nature Link*. URL: https://link-springer-com.ludwig.lub.lu.se/rwe/10.1007/978-94-007-2739-7_64 (visited on 05/12/2026).

[27] H. Faraoun et al. “Elastic properties of binary NiAl, NiCr and AlCr and ternary Ni2AlCr alloys from molecular dynamic and Abinitio simulation”. In: *Computational Materials Science*. Proceedings of the E-MRS 2004 Spring Meeting; Symposium H: Atomic Materials Design: Modelling and Characterization 33.1 (Apr. 2005), pp. 184–191. ISSN: 0927-0256. DOI: 10.1016/j.commatsci.2004.12.011. URL: https://www.sciencedirect.com/science/article/pii/S0927025604003209 (visited on 04/21/2026).

[28] S. K. Mukherjee, P. K. Barhai, and S. Srikanth. “Comparative evaluation of corrosion behaviour of type K thin film thermocouple and its bulk counterpart”. In: *Corrosion Science* 53.9 (Sept. 2011), pp. 2881–2893. ISSN: 0010-938X. DOI: 10.1016/j.corsci.2011.05.024. URL: https://www.sciencedirect.com/science/article/pii/S0010938X11002460 (visited on 04/22/2026).

[29] *Introduction to materials: fundamentals and interactions*. en-US. DOI: 10.1016/B978-0-12-813294-4.00006-6. URL: https://www.sciencedirect.com/science/chapter/monograph/pii/B9780128132944000066 (visited on 05/14/2026).

[30] “Properties of Materials”. en-US. In: *Biomaterials Science*. Academic Press, Jan. 1996, pp. 11–35. DOI: 10.1016/B978-0-08-050014-0.50006-7. URL: https://www.sciencedirect.com/science/chapter/edited-volume/pii/B9780080500140500067 (visited on 05/14/2026).

[31] Klaus A. Moltved and Kasper Planeta Kepp. “The Chemical Bond between Transition Metals and Oxygen: Electronegativity, d-Orbital Effects, and Oxophilicity as Descriptors of Metal–Oxygen Interactions”. In: *Journal of Physical Chemistry C* 123.30 (2019), pp. 18432–18444. ISSN: 1932-7447. DOI: 10.1021/acs.jpcc.9b04317.

[32] *Structure of Organic Compounds*. en-US. DOI: 10.1016/B978-0-12-802444-7.00001-X. URL: https://www.sciencedirect.com/science/chapter/monograph/pii/B978012802444700001X (visited on 05/14/2026).

[33] *Experimental Methodologies for the Characterization of Nanoparticles*. en-US. DOI: 10.1016/B978-0-12-801406-6.00004-2. URL: https://www.sciencedirect.com/science/chapter/monograph/pii/B9780128014066000042 (visited on 04/10/2026).

[34] "Scanning electron microscopy". en-US. In: (Jan. 2024), pp. 36–50. DOI: 10.1016/B978-0-323-90800-9.00128-1. URL: https://www.sciencedirect.com/science/chapter/referencework/pii/B9780323908009001281 (visited on 04/10/2026).

[35] "Surface Micrography and Analysis". en-US. In: *Tribology Series*. Vol. 44. Elsevier, Jan. 2004, pp. 165–220. DOI: 10.1016/S0167-8922(04)80024-5. URL: https://www.sciencedirect.com/science/chapter/bookseries/pii/S0167892204800245 (visited on 04/10/2026).

[36] A. M. Joshua, G. Cheng, and E. V. Lau. "Soft matter analysis via atomic force microscopy (AFM): A review". In: *Applied Surface Science Advances* 17 (Oct. 2023), p. 100448. ISSN: 2666-5239. DOI: 10.1016/j.apsadv.2023.100448. URL: https://www.sciencedirect.com/science/article/pii/S266652392300082X (visited on 05/14/2026).

[37] *Materials and Their Weldability*. en-US. DOI: 10.1016/B978-1-84569-641-2.50004-0. URL: https://www.sciencedirect.com/science/chapter/monograph/pii/B9781845696412500040 (visited on 05/13/2026).

[38] S. Rubeck et al. "Effect of accelerated hydrothermal aging on the durability of Si-based dielectric thin films". In: *Microelectronic Engineering* 264 (Aug. 2022), p. 111858. ISSN: 0167-9317. DOI: 10.1016/j.mee.2022.111858. URL: https://www.sciencedirect.com/science/article/pii/S0167931722001526 (visited on 05/07/2026).

[39] L. Wang, C. Liang, and B. C. Prorok. "A comparison of testing methods in assessing the elastic properties of sputter-deposited gold films". In: *Thin Solid Films* 515.20 (July 2007), pp. 7911–7918. ISSN: 0040-6090. DOI: 10.1016/j.tsf.2007.04.022. URL: https://www.sciencedirect.com/science/article/pii/S0040609007005330 (visited on 04/29/2026).

[40] Tsugutomo Kudoh and Yoh-Ichiro Ogita. "Resistance characteristics to oxidation of the metal-catalyzer for Cat-CVD". In: *Thin Solid Films*. Proceedings of the Fifth International Conference on Hot-Wire CVD (Cat-CVD) Process 517.12 (Apr. 2009), pp. 3443–3445. ISSN: 0040-6090. DOI: 10.1016/j.tsf.2009.01.048. URL: https://www.sciencedirect.com/science/article/pii/S0040609009000510 (visited on 04/29/2026).

[41] Szu-Chia Chien and Wolfgang Windl. "Bond Synergy Model for Bond Energies in Alloy Oxides". en. In: *Journal of The Electrochemical Society* 167.14 (Nov. 2020), p. 141511. ISSN: 1945-7111. DOI: 10.1149/1945-7111/abc6c7. URL: https://doi.org/10.1149/1945-7111/abc6c7 (visited on 05/13/2026).

[42] R. Pretorius, J. M. Harris, and M-A. Nicolet. "Reaction of thin metal films with SiO2 substrates". In: *Solid-State Electronics* 21.4 (Apr. 1978), pp. 667–675. ISSN: 0038-1101. DOI: 10.1016/0038-1101(78)90335-0. URL: https://www.sciencedirect.com/science/article/pii/0038110178903350 (visited on 05/13/2026).

[43] R. H. Dauskardt et al. "Adhesion and debonding of multi-layer thin film structures". In: *Engineering Fracture Mechanics* 61.1 (Aug. 1998), pp. 141–162. ISSN: 0013-7944. DOI: 10.1016/S0013-7944(98)00052-6. URL: https://www.sciencedirect.com/science/article/pii/S0013794498000526 (visited on 05/07/2026).

A AFM image comparison

Following shows the comparison of the AFM height and phase image.

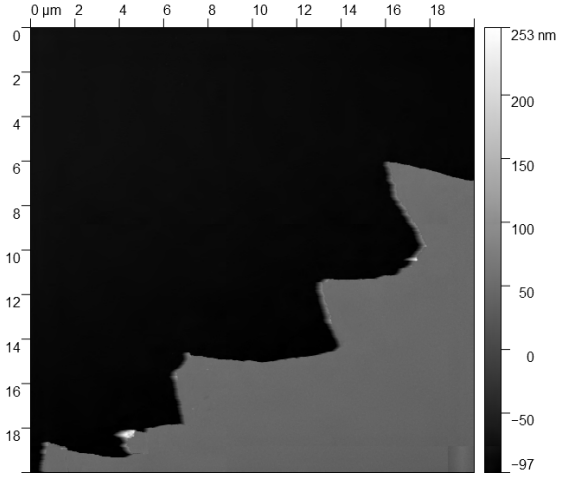

(a) Height image

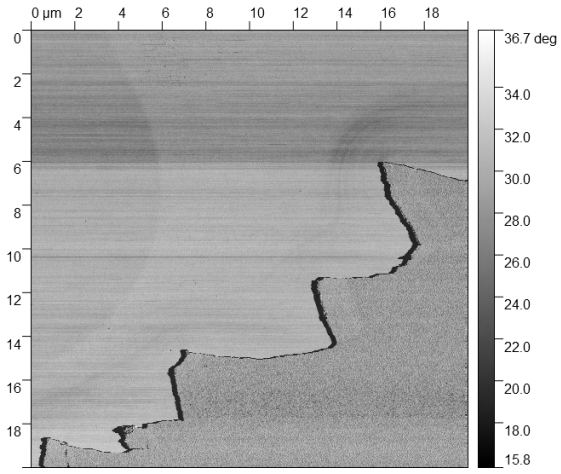

(b) phase image

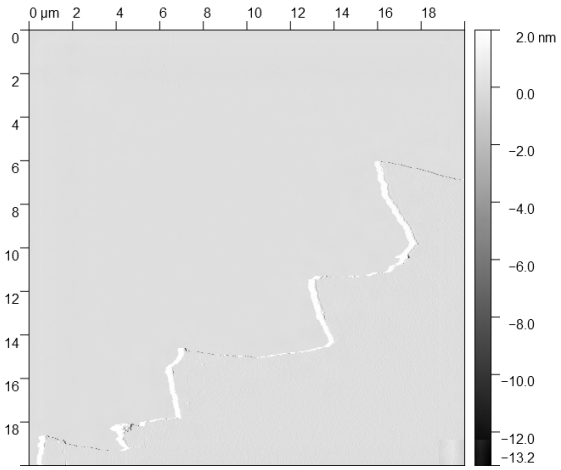

(c) Error for height image

Figure 15: Comparison of AFM topographic height image (a) against phase change image (b). (a) shows high height difference between chromel and silicon wafer. (b) shows additional intermediate layer. Increased brightness of intermediate layer indicates stiffer metal, revealing pre-deposited nickel layer. (c) shows the surface error of the height.